First integrated tephrochronological record for the last ~190 kyr from the Fucino Quaternary lacustrine succession, central Italy

Biagio Giaccio [a, *], Elizabeth M. Niespolo [b, c], Alison Pereira [d, e, f, g], Sebastien Nomade [d], Paul R. Renne [b, c], Paul G. Albert [h], Ilenia Arienzo [j], Eleonora Regattieri [a, k], Bernd Wagner [k], Giovanni Zanchetta [l], Mario Gaeta [m], Paolo Galli[a, n], Giorgio Mannella [l], Edoardo Peronace [a], Gianluca Sottili [a], Fabio Florindo [o], Niklas Leicher [k], Fabrizio Marra [o], Emma L. Tomlinson [p]

[a] Istituto di Geologia Ambientale e Geoingegneria, CNR, Roma, Italy
[b] Department of Earth and Planetary Science, University of California, Berkeley, USA
[c] Berkeley Geochronology Center, Berkeley, USA
[d] Laboratoire des Sciences du Climat et de l'Environnement (CEA-CNRS-UVSQ), Gif-Sur-Yvette, France
[e] École française de Rome, Roma, Italy
[f] Département de Préhistoire du Muséum national d'Histoire naturelle, Paris, France.
[g] Sezione di Scienze Preistoriche e Antropologiche, Dipartimento di Studi Umanistici, Università degli Studi di Ferrara, Ferrara, Italy
[h] RLAHA, University of Oxford, Oxford, UK
[j] Istituto Nazionale di Geofisica e Vulcanologia, Sezione Osservatorio Vesuviano, Napoli, Italy
[k] Institute of Geology and Mineralogy, University of Cologne, Cologne, Germany
[l] Dipartimento di Scienze della Terra, University of Pisia, Pisa, Italy
[m] Dipartimento di Scienze della Terra, University of Roma "La Sapienza" Roma, Italy
[n] Dipartimento di Protezione Civile Nazionale, Roma, Italy
[o] Istituto Nazionale di Geofisica e Vulcanologia, Sezione Roma 1, Roma, Italy
[p] Department of Geology, Trinity College Dublin, Dublin, Ireland

* Corresponding author: biagio.giaccio@cnr.it

Abstract

We present the first integrated tephrochronological study (major and trace elemental glass composition, Sr and Nd isotope analyses, and $^{40}Ar/^{39}Ar$ dating) for the last one tenth (~84 m) of the ~900 m-thick Quaternary lacustrine succession of the Fucino Basin, the largest and probably only Central Apennine intermountain tectonic depression that hosts a continuous lacustrine succession documenting the Plio-Quaternary sedimentary history up to historical times. Major element glass compositions, determined using a wavelength-dispersive electron microprobe (WDS-EMPA), yielded the geochemical fingerprinting needed for a reliable identification of most of the 23 stratigraphically ordered tephra layers under investigation. These include tephra from Italian volcanoes such as Campi Flegrei, Etna, Colli Albani, Ischia,Vico, Sabatini, and undefined volcanic sources in the Neapolitan area and Latium region. The recognition of key Mediterranean marker tephra layers (e.g. X-5 and X-6) is supported by trace element data acquired by Laser Ablation Inductively Couple Plasma Mass Spectrometry (LA-ICP-MS). The Sr and Nd isotope compositions of selected layers where also determined for circumscribing the volcanic source of distal tephra and for supporting correlations with individual eruptive units. We also propose a new, more expeditious covariation diagram (CaO/FeO_{tot} vs Cl) for identifying the volcanic source of trachytic to phonolitic and tephrytic to

phonolitic tephra, that are the most common compositions of pyroclastic rocks from volcanoes of Campania and Latium regions. Finally, we present five new $^{40}Ar/^{39}Ar$ age determinations, including a new, analytically well-supported, and more precise $^{40}Ar/^{39}Ar$ age for the widespread Y-7 tephra, and the first $^{40}Ar/^{39}Ar$ age determinations for one tephra from the Sabatini volcanic district (~126 ka) and one tephra from Neapolitan volcanic area (Campi Flegrei?; ~159 ka). These newly dated tephra are widely dispersed (e.g. Monticchio, southern Italy, Adriatic Sea and Lake Ohrid, Macedonia-Abania) and have thus the potential to become important Mediterranean MIS 5 and MIS 6 tephrochronological markers. Altogether the new geochemical and $^{40}Ar/^{39}Ar$ ages precisely constrain the chronology of the investigated Fucino succession spanning the last ~190 ka. In light of these results and by considering that this sedimentary succession possibly extends back to ~2 Ma, Fucino is likely to provide a very long, continuous tephrostratigraphic record for the Mediterranean area and become a key node in the dense network of tephra correlations of this region.

1. Introduction

Much of our knowledge and understanding of the spatial-temporal variability and mechanisms underlying Quaternary climatic changes, as well as any other time-dependent geological process or phenomenon, rely on high-quality and high-resolution records anchored by precise and accurate time scales. In this framework, distal volcanic ash layers or tephra, ejected into the atmosphere during large explosive eruptions and simultaneously deposited in different stratigraphic successions, have become increasingly relevant to providing critically needed time stamps (e.g. Lowe, 2011). Indeed, tephra are powerful tools for dating and synchronizing natural archives and for mutually transferring information from one record to another, as they are independent of the uncertainties inherent in the comparison of time series that are built with different age models and chronological assumptions (e.g. Scholz and Hoffmann., 2011; Bronk Ramsey et al., 2014). This is an unambiguous precondition for a highly reliable assessment of the temporal relationship and the potential causal connections between disparate processes and events.

The recurrent and long-lasting explosive activity from the peri-Tyrrhenian Quaternary volcanic centers (e.g. Peccerillo, 2005) makes the central Mediterranean region an ideal area for the development of the tephrostratigraphic method (e.g. Wulf et al., 2004, 2012; Munno and Petrosino, 2007; Giaccio et al., 2012, 2013, 2014; Paterne et al., 2008; Zanchetta et al., 2008; Bourne et al., 2010; 2015; Sulpizio et al., 2010;

Smith et al., 2011; Tamburrino et al., 2012; Tomlinson et al., 2012; Insinga et al., 2014; Marchini et al., 2014; Petrosino et al., 2014). Although this potential was exploited in recent years for solving archaeological and palaeoclimatic issues (Zanchetta et al., 2011; Lowe et al., 2012; Giaccio et al., 2015a; Regattieri et al., 2015; 2016; Pereira et al., 2015; Villa et al., 2016), to date, tephrostratigraphic investigations focused mainly on the relatively short interval of the Upper Pleistocene-Holocene, and only very few studies addressed the Early-Middle Pleistocene period (e.g. Karner et al., 1999; Giaccio et al., 2014; Insinga et al., 2014; Petrosino et al., 2014). Moreover, among these records, the oldest ones are generally fragmentary and incomplete, as they often refer to relatively short temporal-stratigraphic intervals with limited or no paleoclimatic information. On the other hand, despite several long climate records have been produced in recent years in the Mediterranean, from continental (e.g. Tzedakis et al., 2006; Wagner et al., 2014; Pross et al., 2015; Sadori et al., 2015) and marine (e.g. Maiorano et al., 2013; Capotondi et al., 2015) realms, a satisfactory synchronization between different archives is still pending, thus keeping the evaluation of leads, lags and timing of propagations of climatic events largely speculative (e.g. Zanchetta et al., 2016).

The identification and study of long and continuous successions where tephrostratigraphy may be successfully applied and joined to multiproxy geochemical and biological data are therefore of paramount importance. Lacustrine successions hosted in Quaternary tectonic basins over the Central Apennine, central Italy, have been shown to fulfill these requirements, having a high potential to give novel insights on the most cogent paleoclimatic and paleomagnetic issues currently under debate (Giaccio et al., 2012, 2015a; Sagnotti et al., 2014; 2016; Regattieri et al., 2015; 2016). Despite of this great potential, many of the Central Apennine outcropping successions are discontinuous and document short chronological intervals.

Among the numerous Plio-Pleistocene intermountain tectonic depressions of the Apennine chain, Fucino Basin is the largest and probably only basin hosting a continuous and thick lacustrine succession of ~900 m thickness documenting the Plio-Quaternary sedimentary history up to the recent historical times (e.g. Giaccio et al., 2015b) (Fig. 1). Furthermore, it is located in a favorable position with respect to the prevailing westerlies and in a good range of distance from many of the peri-Tyrrhenian Italian volcanic centers (100 to 150 km; Fig. 1) to have an almost complete record of distal tephra that are still sufficiently coarse to be dated with useful precision by means of the $^{40}Ar/^{39}Ar$ dating method (e.g. Giaccio et al., 2012; 2013a; 2013b; 2015a; Sagnotti et al., 2014).

In order to explore the tephrochronological and palaeoclimatic potential of this succession, in June 2015 we recovered a ~84 m-long core from the central-eastern Fucino Basin (F1-F3 in Fig. 1). The preliminary results of the multiproxy investigations highlighted the sensitivity of lake sediments to the climatic-environmental changes over the last 190 kyr and documented the presence of a rich tephra record (Giaccio et al., 2015b). In this paper we present the first results of an integrated tephrochronological investigation, including major and trace elements glass composition, Sr and Nd isotope analyses and $^{40}Ar/^{39}Ar$ geochronology of the uppermost ~84 m (~10%) of the ~900 m-long sedimentary infilling of the Fucino Basin.

2. Geological, seismotectonic and stratigraphic framework of the Fucino Basin

The opening and the Plio-Quaternary evolution of the Fucino Basin was driven by the Fucino Fault System (FFS), which is made up by three N110°-140° primary segments (Galadini and Galli, 2000) subtending in their hanging-wall N130°-140° synthetic and antithetic splays (Fig. 1). On the whole, the FFS depicts a semi-graben architecture, with a Plio-Pleistocene lacustrine infilling reaching ~900 m of thickness toward the depocenter as revealed by several commercial and scientific seismic lines (Cavinato et al., 2002; Patacca et al., 2008) (Fig. 1). The results of the preliminary tephra and multiproxy investigations performed on the newly acquired cores F1-F3, along with the revision of the previous data from cores GeoLazio and Telespazio (Fig. 1), suggest that sedimentary basin infill is likely to continuously span the last ~2 Ma (Giaccio et al., 2005b). The FFS is currently active (e.g. Galli et al., 2016a) and responsible for the most devastating earthquake of central Italy (January 13, 1915, Mw 7.0, Io 11 MCS grade; ~33,000 victims). The basin is surrounded by some of the highest reliefs of the Central Apennine, which during recent glacial periods hosted mountain glaciers (e.g. Giraudi and Giaccio, 2015). In historical time the Fucino Basin hosted the Lake Fucinus, which covered a surface area of 150 km^2 until the lake was partially drained under Emperors Claudius and Hadrian (1^{st}-2^{nd} century CE), to be then completely drained by the Torlonia family at the end of the 19^{th} century.

3. Material and methods

3.1. Investigated cores

The tephrostratigraphic investigations have been performed on ash layers from the cores F1-F3 (see drilling strategy and method in Giaccio et al., 2015b) and from two ~30 m-long cores (SP and SPE in Fig. 1), which were drilled for engineering purposes in 2012, ~2 and ~8 km East from F1-F3 drilling site, respectively (Fig. 1). Although this study essentially deals with visible ash layers, tephra detection was also supported by XRF scanning data that mark tephra with prominent peak of K, Rb and/or Sr (Fig. 2), and that occasionally allowed identification of barely visible ash. However, at present no detailed and systematic cryptotephra investigations have been performed on the cores. The tephra have been labeled as Tephra Fucino (TF) followed by a sequential numbering indicating the relative stratigraphic position of each tephra, TF-1 being the uppermost layer.

3.2. $^{40}Ar/^{39}Ar$ Geochronology

$^{40}Ar/^{39}Ar$ geochronology was performed on pristine sanidine or leucite crystals, ranging in size from 150 μm to 2 mm, from five tephra layers (TF-4, TF-5, TF-7, TF-14 and TF-17) in two different laboratories. TF-4, TF-5, TF-7 and TF-17 were dated at the Berkeley Geochronology Center (BGC; Berkeley, USA), whilst TF-7, TF-14 and TF-17 were dated at the Laboratoire des Sciences du Climat et de l'Environnement (CNRS-LSCE; Gif Sur Yvette, France). Weighted mean ages of both the BGC and CNRS-LSCE dates are calibrated to the age of ACs = 1.193 ± 0.001 Ma (Nomade et al., 2005) and the decay constants of Steiger & Jager (1977). A more recent calibration (Niespolo et al., 2016) yields slightly different ages but we retain the previous calibration here for consistency with previous results.

BGC – Two samples were collected from the tephra layer TF-4 (11.68 m and 11.74 m), and one sample from tephra TF-5 (12.00 m), TF-7 (15.40 m), and TF-17 (32.45 m), all from core SP (Fig. 2). Samples were sieved and washed in distilled water in an ultrasonic bath. Sanidine and leucite were separated using a Frantz Isodynamic magnetic separator and heavy liquids. Leucite concentrate from layer TF-5 was cleaned with dilute (5-7%) hydrofluoric acid in an ultrasonic bath for 5 minutes to remove adhering residues, while other samples contained clean sanidine not requiring a hydrofluoric rinse. All samples were finally handpicked to purity. Samples were loaded into a sixteen-pit 18.5-mm aluminium disk: Fucino samples were placed into three large 4.5-mm diameter pits and two smaller 3.18-mm pits; Alder Creek sanidine (ACs) crystals were

loaded into surrounding 3.18-mm pits as a neutron fluence monitor. The disk was irradiated for 0.5 hours at the Cd-lined, in-core CLICIT facility of the Oregon State University TRIGA reactor and labelled irradiation 446PRA. J values of Fucino samples were determined by interpolation of a planar fit to J-values determined from the ACs standard data.

All samples, including ACs standards, were analyzed on a MAP 215-50 mass spectrometer dubbed Nexus, with a Nier-type ion source and an analog electron multiplier detector. Single grains of Fucino samples underwent total laser fusion from a CO_2 laser at 7 Watts of power. ACs samples from small pits were measured by total fusion of 3-grain aliquots. For each sample, blank and air pipette, fifteen cycles were determined for each Ar isotope using peak hopping by magnetic field switching on a single detector. Evolved gases were cooled to ca. -100 to -135 °C using a cryotrap and exposed to a c. 450 °C hot getter to remove reactive gases. For all samples, a mean blank correction was determined using background isotopic measurements analyzed between each single-grain analysis. Blank between sample measurements was stationary over time, and mean values and standard deviations were used to correct the sample and air pipette data. Mass discrimination was determined based on automated analyses of air pipettes between every five single grain analyses (plus intercalated blank) using air pipette data based on a power law correction (Renne et al., 2009) and the atmospheric values of Lee et al. (2006). See the supplementary data in Table S1 for mass discrimination values. Interference corrections were based on the following nucleogenic production ratios: $(^{40}Ar/^{39}Ar)_K = (7.30 \pm 0.92) \times 10^{-4}$; $(^{38}Ar/^{39}Ar)_K = (1.196 \pm 0.013) \times 10^{-2}$; $(^{39}Ar/^{37}Ar)_{Ca} = (7.02 \pm 0.12) \times 10^{-4}$; $(^{36}Ar/^{37}Ar)_{Ca} = (2.702 \pm 0.004) \times 10^{-4}$; $^{36}Cl/^{38}Cl = (2.628 \pm 0.002) \times 10^{2}$.

CNRS-LSCE – Samples of the tephra TF-7 and TF-17, from core SP, and TF-14, from core F1-F3 (Fig. 1), were sieved and washed in water. Clear and unaltered sanidine crystals ranging from 250 μm up to 1 mm in size were handpicked under a binocular microscope. To prevent any groundmass contaminations, crystals were leached for 5 min in dilute (5 to 7%) hydrofluoric acid. For layer TF-7 and TF-17 approximately thirty crystals were chosen and separately loaded in aluminium disks in order to obtain ages on single-grains. In TF-14 the mean size of the crystals was around 250 μm, i.e., somewhat smaller than the two other samples, hence tephra analyses were performed on populations of 6-10 crystals. TF-7, TF-14 and TF-17 were then irradiated for 40 min (IRR 107, J value = 2.2010×10^{-4}), 45min (IRR 119, J value = 3.7440×10^{-4}) and for 60min (IRR 106, J value = 3.579×10^{-4}), respectively, in the β1 tube of the OSIRIS reactor (French Atomic

Energy Commission, Saclay, France). After irradiation, samples were transferred into a copper holder and single crystals from TF-7 and TF-17 were loaded in individual hole, whereas 6-10 crystals per hole were loaded for TF 14. This copper holder was then places into a differential vacuum Cleartran© window. Sanidines were then fused using a Synrad CO_2 laser (c.a 25 Watts) and the quantities of the argon isotopes (^{40}Ar, ^{39}Ar, ^{38}Ar, ^{37}Ar and ^{36}Ar) were measured using a VG 5400 mass spectrometer equipped with a single ion counter (Balzers SEV 217 SEN). Each Ar isotope measurement consisted of 20 cycles of peak switching of the argon isotopes. J values were obtained by co-irradiation of Alder Creek sanidines (ACs-2, Nomade et al., 2005). Full analytical details are provided in Supplementary Table S2. Mass discrimination was assessed by analysis of air pipette throughout the analytical period, and was calculated relative to a $^{40}Ar/^{36}Ar$ ratio of 298.56 (Lee et al., 2006). Procedural blanks were measured every two or three unknown measurements. For a typical 10 min static blank, the backgrounds were generally about $3.0–4.0 \times 10^{-17}$ and $6.0–7.0 \times 10^{-19}$ mol for ^{40}Ar and ^{36}Ar, respectively. The nucleogenic production ratios used to correct for reactor-produced Ar isotopes from K and Ca are reported in the supplementary dataset.

3.3. Major and minor element compositions

Major and minor oxide element compositions were determined on micro-pumice fragments and/or glass shards (grain size >125 μm), from 20 out of 22 tephra in core F1-F3, 6 tephra in core SP, 6 tephra in core SPE (Fig. 2) and, for comparison, from the proximal Baccano Lower Unit of the Sabatini volcanic district (Sottili et al., 2010). The analyses of the 32 samples were carried out at the Istituto di Geologia Ambientale e Geoingegneria of the Italian National Research Council (IGAG-CNR) (Rome, Italy) using a Cameca SX50 electron microprobe equipped with a five-wavelength dispersive spectrometer. Operating conditions were set to 15 kV accelerating voltage; 15 nA beam current; 10-15 μm beam diameter; 20 s per element counting time; Wollastonite (Si and Ca), corundum (Al), diopside (Mg), andradite (Fe), rutile (Ti), orthoclase (K), jadeite (Na), phlogopite (F), potassium chloride (Cl), barite (S), and metals (Mn) were used as standards. The Ti content was corrected for the overlap of Ti-Kα peaks. In order to evaluate the accuracy of the electron microprobe analyses, three international secondary standards (Kakanui augite and rhyolite RLS132 glasses from the United States Geological Survey) were measured prior of each analytic run. Test results are reported in Supplementary Table S3.

3.4. Trace elements

Trace element analyses were performed on glasses of the Fucino tephra TF-12, TF-13 (from core F1-F2; Fig. 2) and TF-17 (from core SP; Fig. 2) and, for comparison, of the OH-DP-0624 tephra occurring in MIS 6 sediments of the DEEP site record of Lake Ohrid (Leicher et al., 2016). The analyses were performed using a Thermo Scientific iCAP Qc ICP-MS coupled to a Teledyne Photon Machines Analyte G2 193 nm eximer laser ablation system with a HelEx II two-volume ablation cell at the Department of Geology, Trinity College, Dublin. A spot size of 25 μm was used owing to the size of the ash particles and glassy areas available for analysis. The repetition rate was 5 Hz and the count time was 40 s (200 pulses) on the sample and 40 s on the gas blank (background). The ablated sample was transported in He gas flow (0.65 L min^{-1}) with additional N_2 (5 ml min^{-1}) via a signal smoothing device. Concentrations were calibrated using NIST612 with ^{29}Si as the internal standard. Data reduction was performed using Iolite 2.5 and portions of the signal compromised by the ablation of microcrysts and resin-filled voids were excluded. Accuracies of ATHO-G and StHs6/80-G MPI-DING glass analyses are typically ≤5% for V, Rb, Sr, Y, Zr, Ba, La, Ce, Nd, Eu, Dy, Er, Th; <10% for Nb, Pr, Sm, Gd, Yb, Hf, U and <15% for Ta. Reproducibility of the ATHO-G analyses were typically < 5% RSD for all trace elements with the exception of Sm, Eu, Yb (<6%) and V (≤8%). For full details of all the secondary standard analyses run alongside with the Fucino tephra glass data refer to the Supplementary Table S4.

3.5. Strontium (Sr) and neodymium (Nd) isotopes

Sr and Nd isotope compositions were determined by thermal ionization mass spectrometry at the Istituto Nazionale di Geofisica e Vulcanologia, Osservatorio Vesuviano (Naples, Italy), using a ThermoFinnigan Triton TI multicollector mass spectrometer on glass-rich samples from eight Fucino tephra (TF-7, TF-10, TF-12, TF-13, TF-14, TF-16 and TF-20 in core F1-F3 and TF-17 in core SP; Fig. 2). Sr-Nd isotope analysis were also performed, for comparison, on the tephra POP1 and POP2a from MIS 5 sediments of Sulmona Basin (Giaccio et al., 2012) and the MIS 6 tephra OH-DP-0624 from the DEEP site record of Lake Ohrid (Leicher et al., 2016). Most analyses were performed on glass shards, but for sample TF-7 isotope compositions were obtained on feldspar crystals selected under binocular microscope. 0.2 g of sample were

leached several times with cold 6 N HCl for 10 min, and then rinsed in pure Milli Q® H_2O. After dissolution, Sr and Nd were separated by conventional ion-exchange chromatographic techniques. The Sr blank was on the order of 0.1 ng during the period of chemistry processing. Measured $^{87}Sr/^{86}Sr$ and $^{143}Nd/^{144}Nd$ isotope ratios were normalized for within-run isotopic fractionation to $^{86}Sr/^{88}Sr$ =0.1194 and $^{146}Nd/^{144}Nd$ =0.7219, respectively. The mean measured values of $^{87}Sr/^{86}Sr$ for NIST-SRM 987 and of $^{143}Nd/^{144}Nd$ for La Jolla were 0.710220 ± 0.000019 (2σ, N=122) and 0.511845 ± 0.000010 (2σ, N=42), respectively. The external reproducibility 2σ is calculated according to Goldstein et al. (2003). Sr and Nd isotope ratios have been normalized to the recommended values of NIST SRM 987 ($^{87}Sr/^{86}Sr$ =0.71025) and La Jolla ($^{143}Nd/^{144}Nd$ =0.51185) standards, respectively.

4. Results

4.1. Stratigraphy, major and trace element glass composition and Sr and Nd isotope ratios

Lithology in the investigated cores F1-F3, SP, and SPE, is rather homogeneous and is mainly represented by fine grained lacustrine sediments constituted of grey calcareous marl with a variable proportion of clay and organic matter. The vertical lithological variability is schematically summarized in Figure 2. Each core contains a variable number of tephra that, based on their diagnostic features (i.e., geochemical composition, lithological characters and stratigraphic order), made it straightforward to correlate among them (Fig. 2). In particular, the blackish TF-4 and TF-5 tephra, with their peculiar lithological features, significant thickness, coarse-grain size and stratigraphic proximity, form a couple of markers for a reliable core correlation. TF-4 in SP actually displays a more evolved chemical composition (higher SiO_2 and A_2O_3 and lower MgO, CaO and FeO) compared with the equivalent layers in core SPE and F1-F3 (see Supplementary Table S3). However, its correlation to the equivalent layers occurring in cores SPE and F1-F3 is warranted by compelling lithological and stratigraphic evidence and therefore the chemical composition difference can be arguably interpreted as an expression of the chemical variability of the tephra.

By using the tephra as tie points, we then build a unique, ~84 m-long composite tephrostratigraphic section, in which the tephra depths are the same as tephra in the most complete and long core F1-F3 (Fig. 2). This results in a total of 21 visible tephra and one cryptotephra (TF-1) spanning the last 190 kyr, or the interval from late Marine Isotope Stage (MIS) 6 to MIS 1 (Giaccio et al., 2015b; Fig. 2). In addition to these 22

ordered layers, we recognize the TF-22 tephra, which was only found within the SPE core (Fig. 2) and thus cannot be precisely placed in composite section. However, if considering that in core SPE the tephra TF-22 is at depth of 29.25 m, (ii) that the tephra TF-15 in cores SPE and F1-F2 is at the depths of 17.35 m and 66.04 m, respectively (Fig. 2), and (iii) assuming that depth difference of TF-15 in cores SPE and F1-F2 – which is a difference in sedimentation rate between the two drilling sites – is projected linearly (i.e., 29.25 : x = 17.35 : 66.04), the depth of TF-22 should roughly correspond to ~112 m at the F1-F3 location (Fig. 2).

Major element composition of the glass from the 23 Fucino tephra is compositionally heterogeneous, including foidite, tephrite, potassic phono-tephrite, tephri-phonolite to phonolite, trachyte and phonolite and Na-alkaline trachyandesite to trachyte (Fig. 3a; full analytical data are given in Supplementary Table S3).

Trace element analyses of volcanic glasses from the three tephra layers characterized here, TF-12, TF-13 and TF-17, reveal varying levels of incompatible trace element enrichment (Fig. 3b; Supplementary Table S4), while sharing broadly consistent ratios of High Field Strength Elements (HFSE) to Th (i.e., TF-12: Nb/Th = 2.1 ± 0.2, Zr/Th = 12.6 ± 1.1 [2 s.d.]; TF-13: Nb/Th = 2.1 ± 0.1, Zr/Th = 11.9 ± 1.0 [2 s.d.]; TF-17: Nb/Th = 2.0 ± 0.1, Zr/Th = 11.6 ± 1.5 [2 s.d.]). At a trace element level the, TF-12 trachytic glasses are the most homogeneous of the three investigated tephra layers, yet some incompatible trace element variation exists (i.e., 19.7-27.5 ppm Th; 255-354 ppm Zr; Fig. 3b), the most significant heterogeneity is observed in Ba (1862-549 ppm) and Sr (965-423 ppm) which are negatively correlated to increasing incompatible element concentrations (i.e., HFSE). The incompatible trace element concentrations observed in the trachytic glasses of TF-13 are extremely heterogeneous (i.e., 34-89 ppm Th; 453-1060 ppm Zr; Fig. 3b); with these levels of enrichment far exceeding those observed in the TF-12 and TF-17 glasses (Fig., 3b), these highly evolved glasses (Zr/Sr = 10.9 - 354) show particularly low concentrations of Ba (9-2 ppm) and Sr (42-3 ppm) undoubtedly relating to K-feldspar fractionation. Trace element concentrations of the TF-17 glasses are heterogeneous (i.e., 17.5-36.2 ppm Th; 224-399 ppm Zr; Fig.3b), consistent with significant major element variation in this tephra (Fig.3a; Supplementary Table S4).

The Sr and Nd isotope compositions from the selected Fucino tephra (TF-7, TF-10, TF-12, TF-13, TF-14, TF-16, TF-17 and TF-20) and those from some of their potential correlatives (POP1, POP2a and OH-DP-0624) range from ~0.7068 to ~0.7105 and ~0.51248 and ~0.51212, respectively (Tab. 1). $^{87}Sr/^{86}Sr$ and $^{143}Nd/^{144}Nd$ are correlated and describe a regular trend with increasing $^{87}Sr/^{86}Sr$ and decreasing $^{143}Nd/^{144}Nd$

(Fig. 4). However, this does not apply to sample OH-DP-0624, which, although strongly leached, yielded an inconsistent $^{87}Sr/^{86}Sr$ value (~0.710483), likely because of alteration with respect to the Nd isotope composition of ~0.512495 (Table 1).

4.2. $^{40}Ar/^{39}Ar$ geochronology

Analytical details for each experiment are given in the supplementary dataset (Tables S1 and S2). Results are presented in Figure 5 as probability diagrams (Deino and Potts, 1990). The weighted mean ages for combined laboratory results and those from CNRS-LSCE are calculated using IsoPlot 3.0 (Ludwig, 2001); data solely from BGC analyses were processed using Mass Spec (A. Deino, BGC). Uncertainties are reported at 2σ (95% of confidence interval), including J uncertainty, throughout the text.

TF-4 – Two sub-samples from tephra TF-4 (11.68 m and 11.74 m depth in core SP; Fig. 2) were first analyzed separately. Sample SP-11.68 m yielded a weighted mean age of 41.8 ± 12.0 ka from 45 out of 46 grains. SP-11.74 m yielded a weighted mean age of 47.0 ± 9.6 ka from 42 out of 53 grains. Grains were excluded from this age calculation due to low percent radiogenic ^{40}Ar ($\%^{40}Ar^*$) or negative ages lying clearly outside of the age probability histogram. The ages of the two subsamples are indistinguishable and were thus combined to yield a weighted mean age of 45.0 ± 7.5 ka (MSWD = 0.6, P = 1.0) from 87 out of 99 analyses on sanidine crystals (Fig. 5).

TF-5 – Sample TF-5 yielded a weighted mean age of 39.4 ± 2.0 ka (MSWD = 1.0, P = 0.4) from 51 out of 53 leucite grains (Fig. 5). While at the 95% confidence interval, this age is not necessarily younger than the age of TF-4 deposited above it in the core, it is also possible that this age is spuriously young due to slight alteration of leucite. Leucite grains from TF-5 had a foggy chalky texture and required a cleaning with dilute HF to remove adhering residues. Alteration of leucite mineral surfaces may have led to minor $^{40}Ar^*$ loss resulting in a spuriously young age.

TF-7 – 19 and 53 crystals were dated in the CNRS-LSCE and the BGC laboratories, respectively. The sample analysed at CNRS-LSCE provided a multimodal probability diagram, highlighting three populations (Fig. 5). The youngest population is homogeneous, including 14 out of the 19 dated crystals. The weighted mean age determined for this tephra layer is 56.0 ± 1.0 ka (MSWD = 0.4 and P = 1.0). The $^{40}Ar/^{36}Ar$

intercept demonstrated by the related inverse isochron (i.e., 299.3 ± 3.4) is equivalent to the atmospheric ratio of 298.56.

The sample analyzed at BGC also confirmed a high content of xenocrysts accounting for significant removal of analyses from the final weighted mean age, which is 62.1 ± 13.0 ka from 12 out of 53 grains of sanidine Fig. 5). The 12 youngest crystals represent a single population that is statistically distinct (MSWD = 1.04, P = 0.4) from the entire population (MSWD = 37.62, P = 0).

The results from the two labs are indistinguishable at 95% confidence and thus combined to obtain a final weighted mean age of 56.1 ± 1.0 ka (MSWD = 0.7, P= 0.9; Fig. 5).

TF-14 – Thirteen populations of 6-10 sanidine crystals were measured. The probability diagram obtained is a Gaussian curve (Fig. 3) highlighting a homogenous statistical juvenile population of crystals. The corresponding weighted mean age is 126.4 ± 1.0 ka (MSWD = 0.1 and P = 1.0). The inverse isochron demonstrates a $^{40}Ar/^{36}Ar$ ratio (299.4 ± 8.0) equivalent within uncertainties to the atmospheric ratio (Table S2).

TF-17 – 12 and 54 crystals were dated at the CNRS-LSCE and the BGC laboratories, respectively. The twelve crystals measured at CNRS-LSCE provided a multimodal probability diagram, highlighting contamination by xenocrysts (Fig. 5). The youngest population, of 7 out of 12 analysed grains, allowed us to calculate a weighted mean age of 158.6 ± 2.6 ka (MSWD = 0.4 and P = 0.9). The inverse isochron confirms the absence of excess argon within the crystals with a $^{40}Ar/^{39}Ar$ initial ratio of 299.5 ± 2.2.

28 out of 54 sanidine crystals dated at BGC yielded a weighted mean age of 166.6 ± 15.8 ka (MSWD = 1.0, P = 0.5, Fig. 5). Xenocrysts, samples with distinctly negative ages, and crystals that fell outside of a statistically distinct population were excluded from this age calculation. This result is statistically indistinguishable from that obtained at CNRS-LSCE. The data from both labs were once again combined to obtain a weighted mean age of 158.8 ± 3.0 ka (MSWD = 0.9, P= 0.7, n/N: 35/66; Fig. 5).

5. Discussion

5.1. Volcanic source fingerprinting: a new discrimination diagram

The relatively wide compositional spectrum of the major element composition of the 23 Fucino tephra reflects different volcanic sources. Specifically, in a total alkali versus silica (TAS) classification diagram

(Le Maitre, 2002), three main composition groups can be distinguished: (*i*) foidite (TF-4, TF5, TF-8 and TF-9); (*ii*) Na-alkaline trachyandesite to trachyte (TF-3a and TF-3b) and (*iii*) potassic trachyte-phonolite to tephry-phonolite and phono-tephrite, which includes all the remaining 17 tephra (Fig. 3a).

The first two compositional groups are rather peculiar and thus allow a straightforward identification of their volcanic sources. Within the framework of the Italian Quaternary volcanic record and the chronology of the first group of layers TF-4, TF5, TF-8 and TF-9 (i.e., MIS 3 to MIS 5-MIS 4 transition, Fig. 2), foiditic pyroclastic rocks are a prerogative of the Colli Albani volcanic district (e.g. Giaccio et al., 2013a) (Fig. 3a). Similarly, the Na-alkaline affinity of the second group, including benmoreites, trachyandesite and trachyte terms (Fig. 3a), are distinctive of the Mont Etna rocks (e.g. Corsaro et al., 2013 and references therein) (Fig. 3a).

Discriminating the individual volcanic sources of the third and larger compositional group of tephra is definitely a challenging task. Indeed, the TAS classification diagram is no longer helpful, since most of the compositions of these tephra lie in a field which overlaps seven different volcanic sources; i.e., Ischia, Campi Flegrei, Somma-Vesuvius, Roccamonfina, Mt. Sabatini, Vico and Vulsini (Fig. 3a). In terms of incompatible trace elements, although the ratios of HFSE to Th of the analysed tephra appear to correspond with those determined from proximal tephra deposits erupted by the Campanian volcanoes (Fig. 3b), the lack of trace element data acquired with LA-ICP-MS on glass from the pyroclastic products of many of the Latium volcanoes does not allow an exhaustive comparison, thus limiting the use of this kind of data for discriminating the volcanic sources at this time.

Conversely, Sr and Nd isotope compositions appear to offer a more effective tool for discriminating the volcanic sources of the third group of tephra. Based on the available literature data (e.g. e.g. Conticelli et al., 1997, 2009; De Astis et al., 2004; D'Antonio et al., 1999, 2007; Boari et al., 2009a, 2009b; Di Renzo et al., 2007, 2011; Brown et al., 2014; Del Bello et al., 2014; Gaeta et al., 2016; Sottili et al., submitted), it is possible to circumscribe two source areas for the Fucino tephra. One is the Campanian region, characterized by volcanic products with relatively low $^{87}Sr/^{86}Sr$ and high $^{143}Nd/^{144}Nd$, and the other is the Latium region which features emission of volcanics with higher Sr isotope ratios and lower Nd isotope ratios. On this basis, layers TF-7, TF-10, TF-12, TF-13 and TF-17 – as well as the tephra POP1, POP2a and OH-DP-0624 from the other successions here analysed for comparison purposes – can be attributed to Campanian volcanism,

while TF-14, TF-16 and TF-20 to the Latium volcanoes (Fig. 4). Furthermore, isotope data distinguish among the different volcanic sources of the Campania region. Indeed, while TF-7 has an isotope signature typical of the Ischia volcanoes (e.g. Brown et al., 2014), the other Campanian tephra have isotopic compositions consistent with those of Campi Flegrei pyrlocastic products (e.g. D'Antonio et al., 1999, 2007; Di Renzo et al., 2011; Brown et al., 2014).

However, major element compositions constitute the primary and larger dataset for distal tephra, and thus attempts to discriminate the volcanic sources of the potassic trachyte-phonolite to tephry-phonololite and phono-tephrite glass from distal tephra on this basis would be pivotal for tephrostratigraphic purposes. Some recent studies pointed out that Cl content in the glass of relatively differentiated Italian potassic trachyte-phonolite and tephri-phonolite tephra can provide an useful diagnostic criteria for distinguishing their volcanic source (Giaccio et al., 2014; Palladino et al., 2014), with rocks from Latium volcanoes having substantially lower Cl than Campanian tephra (i.e., <0.2 wt% and >0.3-1.0 wt%, respectively). Another discriminating geochemical criteria is the CaO/FeO ratio, especially for distinguishing the trachytes-phonolites erupted from the Campanian volcanoes; Campi Flegrei, Ischia and Somma-Vesuvius. A general increase in this ratio can indeed be observed in the glasses from Ischia to Campi Flegrei to Somma-Vesuvius (Fig. 6). Therefore, we plotted in a Cl vs. CaO/FeO diagram the WDS and EDS glass compositions relative to the Italian potassic trachyte-phonolite and tephri-phonolite from literature (Santacroce et al., 2008; Smith et al., 2011; Tomlinson et al., 2012; 2014; Giaccio et al., 2014; Marra et al., 2014; Palladino et al., 2014), representative of the compositions of the proximal products, together with the composition of the analysed tephra. This plot allows recognition of well-defined and distinguished fields, one for each volcanic source (Fig. 6).

The similarly, very low (~0.1 wt%), content of Cl in primitive glass from both Campi Flegrei and Latium volcanic products (e.g. Gaeta et al., 2009; Esposito et al., 2011) suggests that the observed differences between these two volcanic districts, shown in the Cl vs CaO/FeO diagram (Fig. 6), should be acquired during the magma differentiation processes. Late crystallization of apatite in the Campi Flegrei magmas (Fowler et al., 2007), is a plausible mechanism for explaining the high concentration of Cl observed in the glass from the most evolved Campi Flegrei rocks. Otherwise, apatite occurs in primitive magmas of the

Roman Province suggesting that the late crystal fractionation of this phase would have produced Cl-poor differentiated magmas (e.g. Palladino et al., 2001; Gaeta et al, 2006; Gozzi et al., 2014; Masotta et al., 2016).

The Cl-rich products of Somma-Vesuvius, Campi Flegrei and Ischia (Fig. 6) show significant variations of the CaO/FeO ratio that cannot be due to differences in the stability of clinopyroxene and magnetite in primitive and differentiated magmas (Shea et al, 2009; Fabbrizio and Carroll, 2008; Pichavant et al., 2014; Granati et al., 2014). More likely, a key role in determining the observed variation of the CaO/FeO ratio is played by the plagioclase fractionation. The stability of the Ca-rich plagioclase in the Campi Flegrei magmas is suggested by several lines of evidences: (*i*) the MELT simulation starting from the primitive compositions (Flowers et al., 2007), (*ii*) its occurrence in the experimental products (Fabbrizio and Carroll, 2008; Granati et al., 2014) and (*iii*) its occurrence in the juvenile products of the largest, caldera forming, Campi Flegrei, Campanian Ignimbrite eruption (e.g. Civetta et al., 1997). Otherwise, experiments on the primitive compositions of Somma-Vesuvius rocks reveal that the Ca-rich plagioclase is unstable (Pichavant et al, 2014) and it is only found as an accessory phase in mafic rocks, such as in the 1906 tephra (<1 %, Santacroce et al., 1993). Therefore, the early fractionation of plagioclase and the consequent decrease of calcium in the differentiated magmas of Campi Flegrei, and possibly Ischia, on one hand, and the instability of the Ca-rich plagioclase in Somma-Vesuvius magma, on the other, can be considered as the main factors underlying the observed variability of the CaO/FeO ratio through the Campanian volcanoes. Moreover, the CaO content of the Somma-Vesuvius magmas is probably buffered at high calcium contents by the carbonate assimilation process (e.g. Jolis et al., 2015).

In summary, the information deduced from the TAS diagram (Fig. 3), Sr and Nd isotopes (Fig. 4) and the new Cl vs. CaO/FeO (Fig. 6) diagrams allow us to ascribe the various tephra to different sources as summarized in Table 2. On this basis, the tephra TF-10, TF-11, TF-12, TF-13 and TF-17 should be ascribed to Campi Flegrei. However, so far, the oldest documented Campi Flegrei activity is dated to ~78 ka (Scarpati et al., 2013). Therefore, at this stage we prefer to cautiously ascribe these tephra to an undefined source in Neapolitan volcanic area, here intended as the area which includes Campi Flegrei, Ischia, Procida and Somma-Vesuvius volcanoes.

With respect to the last group in Table 2, the contradictory indications inferable from the Sr-Nd isotope data and from the Cl vs CaO/FeO diagram do not allow the attribution of the tephra TF-18/19, TF-20 and TF-22

to a specific volcanic source (see details in the following section 5.2., and specifically in sub-section 5.2.8.). This group of tephra has been therefore ascribed to a Latium-undefined volcanic source.

The overall chronological framework provided by the new $^{40}Ar/^{39}Ar$ ages (Fig. 5), the preliminary MIS stratigraphy (Fig. 2), and the identification of volcanic sources allow us to geochemically correlate individual tephra to specific proximal eruptive successions or units or, alternatively, to known distal tephra which may not be well identified in their proximal setting, as is discussed in the following section.

5.2. Individual tephra correlation

5.2.1. Campi Flegrei (TF1-1, TF-2 and TF-6)

TF-1. It is the youngest and the only recognized cryptotephra (Fig. 2). The trachyte to phonolite composition of glass from TF-1 straddles the glass from the pyroclastic products of the post-15 ka activity of the Campi Flegrei (Smith et al., 2011), which is subdivided in three main eruptive phases separated by discrete periods of quiescence (Di Vito et al., 1999). In particular the glass from TF-1 has a chemical composition similar to the products of Epoch 2 (~9.6-9.1 ka) and Epoch 3 (5.5-3.5 ka), and to some extent of the end of Epoch 1 (15-10.6 ka) (Fig. 7a). However, its position in the mid-early Holocene – as depicted by the low-resolution $\delta^{18}O$ record and the high-resolution profile of the Ca content (Fig. 2) – restricts the correlation to the Epoch 2. Among the few eruptions that occurred at Campi Flegrei during this short eruptive phase of activity, the composition of TF-1 overlaps that of the glass from the Sartania 1, Pigna San Nicola, Sartania 2 and San Martino units (Fig. 7a), with the second representing the largest event of the Epoch 2 (e.g. Smith et al., 2011). In particular several glass shards from TF-1 have a relatively high content of CaO, MgO and FeO which is a peculiar, distinctive geochemical feature of the glass from Sartania 1 (Fig. 7a). The second, most evolved group of composition is instead undistinguishable from that of the Pigna San Nicola, Sartania 2 and San Martino (Fig. 7a). TF-1 also contains glass shards with an intermediate compositions (SiO_2 at ca 56 wt%, total alkali at ca 11 wt%) that, while are out of the documented range of variability of the Campi Flegrei tephra of Epoch 2 (Fig. 7a), are rather common in the products of the Epoch 1. However, due to its position well within the Holocene and the relatively high sedimentation rate of the succession, we are inclined to exclude that TF-1 could be derived from the contribution of both Epoch 1 and Epoch 2 activity, that are separated by at least 1 kyr-long phase of quiescence ((Di Vito et al., 1999; Smith et al., 2011). On the

other hand, this could suggest that the Campi Flegrei tephra of Epoch 2 also comprises intermediate compositions, that arguably, due to the incompleteness (erosion, spatial variability of the deposition of the eruptive sub-units) and/or limited expositions of the sections in proximal setting, have not still been documented.

This cluster of eruptions, from the oldest Sartania 1 to the youngest San Martino, occurred in a very narrow time span, with modelled calibrated radiocarbon ages spanning between 9500-9654 cal BP (Sartania), 9201-9533 cal BP (Pigna San Nicola) and 9026-9370 cal yr BP (San Martino) (Smith et al., 2011). Therefore, by considering its wide chemical composition spectrum, it is likely that TF-1 cryptotephra resulted from the fallout of Sartania 1 eruption and from at least another following eruption among Pigna San Nicola, Sartania 2 and San Martino. In this perspective we can thus conservatively attribute to the TF-1 layer an age comprised between 9.7 and 9.0 ka.

TF-2. The relatively wide compositional spectrum, from trachyte to phonolite-tephriphonolite, of the glass from TF-2, coupled with its climatostratigraphic position in the late part of MIS 2 (Fig. 2), allow us to correlate this Campi Flegrei tephra to the caldera forming Neapolitan Yellow Tuff (NYT) eruption (Fig. 7b). The NYT is dated by $^{40}Ar/^{39}Ar$ at 14.9 ± 0.4 ka (Deino et al., 2004) and 14.5 ± 0.4 ka (Galli et al., 2016b) or at 14,320–13,900 by Bayesian modelling of ^{14}C ages (Blockley et al., 2008). It is a widespread Late Glacial tephra that falls in the middle of the Bølling-Allerød interstadials, or Greenland interstadial 1, (e.g. Siani et al., 2004; Lane et al., 2015) and that can be traced from southern Mediterranean marine and terrestrial areas (e.g. Siani et al., 2004; Munno and Petrosino, 2007) into eastern and northern Europe (e.g. Schmidt et al., 2002; Lane et al., 2011; Lane et al., 2015).

Besides the NYT, other Campi Flegrei tephra chronologically compatible for a correlation with TF-2 include the Tufi Biancastri (16.1 ± 0.2 ka; sample OCF 9602 in Tomlinson et al., 2012) and Lagno Amendolare (15963-15321 cal PB; Andronico, 1997). However, both pyroclastic deposits have a much more homogeneous composition (Wulf et al., 2008; Tomlinson et al., 2012) and share with TF-2 and NYT only the most evolved components (Fig. 7b). We can thus reasonably exclude these alternative correlations. On the other hand, in Adriatic Sea core PRAD 1-2 were recognized four tephra layers (PRAD 218, PRAD 268, PRAD 324 and PRAD 404) that are chemically indistinguishable among them and with NYT (Bourne et al., 2010). However, according to the high-resolution profile of the Ca content, which has been related to the

authigenic precipitation of calcite and thus considered a proxy of the lake primary productivity and temperature (Giaccio et al., 2015b), the TF-2 falls in the middle of an interstadial phase at end of the MIS 2 (e.g. see in Fig. 2) which can be arguably interpreted as the expression of the Bølling-Allerød interstadials. Therefore, in spite of the unresolved issue of the four NYT-like layers in core PRAD 1-2, the consistent climatostratigraphic position of TF-2 supports the proposed correlation with NYT.

TF-6. This tephra occurs in MIS 3, ~3 m below the Colli Albani tephra TF-5, dated to 39.4 ± 2.0 ka, and ~30 cm above the Ischia tephra TF-7, dated to 56.1 ± 1.0 ka (Figs. 2 and 5). This allows us to correlate TF-6 to the pre-Campanian Ignimbrite (pre-CI) phase documented at the Trefola Quarry (Orsi et al., 1996) spanning 59–39 ka (Pappalardo et al., 1999).

The $^{40}Ar/^{39}Ar$ age of the lowermost outcropping Trefola unit (Tla, 58.9 ± 1.8 ka), appears consistent with the age of TF-6, which, due to its close stratigraphic proximity with the underlying Ischia tephra, within uncertainty, could be conceivably considered the same of TF-7. Glass composition supports the correlation, but due to the geochemical similarities between Tla, Tlc and, partially, Tlf (Fig. 7c), an individual correlation is currently slightly ambiguous; even though the Tlc unit seems to be the most reasonable equivalent based on the diagram Na_2O vs CaO (Fig. 7c). Similarly to TF-1, TF-6 shows a compositional spectrum wider then its potential correlative, which we interpret in the same way.

5.2.2. Undefined source from the Neapolitan volcanic area (TF-10, TF-11, TF-12, TF-13 and TF-17)

TF-10, TF-11, TF-12 and TF-13. The climatostratigraphic position – at the end of MIS 5c (TF-10), in MIS 5c (TF-11 and TF-12) and in MIS 5d (TF-13) sub-stages (Fig. 2), the major and trace element glass composition and the Sr-Nd isotopic compositions of these four layers match that of the tephra POP1, POP2a, POP3 and POP4 found in the nearby basin of Sulmona (Giaccio et al., 2012; Regattieri et al., 2015) (Figs. 7d, 8a, 8b, 8c, 9a and 9b; Tab. 1). POP1 was correlated to the C-22 marine marker tephra of the Tyrrhenian Sea, while POP3 and POP4 were correlated with the widespread X-5 and X-6 markers, first reported in the sediments of the Ionian Sea (Keller et al., 1978). POP1, POP3, and a sample of X-6 tephra in Tyrrhenian Sea have been directly dated by $^{40}Ar/^{39}Ar$ method to 92.4 ± 4.6 ka (2σ), 106.2 ± 1.3 ka (2σ) (Giaccio et al., 2012) and 108.9 ± 1.8 ka (1σ) (Iorio et al., 2014), respectively.

Although the definitive stratigraphic proof has not yet been acquired, these markers are commonly related to the Campi Flegrei area (e.g., Paterne et al., 2008; Wulf et al., 2012). From this perspective, our $^{87}Sr/^{86}Sr$ and $^{143}Nd/^{144}Nd$ ratios (Table 1; Fig. 4) provide the first isotopic evidence that confirms an origin in the Neapolitan volcanic area. Results show that POP1 and TF-10 are both characterized by $^{87}Sr/^{86}Sr$ of ~0.7069 and $^{143}Nd/1^{44}Nd$ of ~0.5125 (Tab. 1). The oldest TF-12 tephra and TF-13 (X-6) are featured by highest Sr isotope ratio (0.707318 and 0.707241, respectively) and relatively low $^{143}Nd/^{144}Nd$ (0.512476 and 0.512497, respectively). These isotopic compositions are similar to those of the pre-CI samples analyzed by Pabst et al. (2008) and D'Antonio et al. (2007).

Equivalent layers of TF-10/C-22, TF-11, TF-12/X-5 and TF-13/X-6 have been recognized in a number of lacustrine – e.g. Lake Ohrid, Macedonia-Albania (OH-DP-0435=TF-13/X-6; Leicher et al., 2016), Monticchio Lake (TM-23-11=TF-10/C-22, TM-24b=TF-11, TM-25=TF-12/X-5, TM-27=TF-13/X-6; Wulf et al., 2012) – marine, – e.g. Adriatic Sea (PRAD-2517=TF-10/C-22 and PRAD-2812=TF-13/X-6; Bourne et al., 2015), Tyrrhenian Sea (CET1-10/14=TF-10/C-22, CET1-15=TF-11, CET1-18=TF-12; Petrosino et al., 2016) – and sub-aerial – e.g. Cilento and Valle del Crati, southern Italy (TF-12/X-5 and TF-13/X-6; Donato et al., 2016) – successions of the central Mediterranean (Figs. 7d, 8a, 8b, 8c, 9a and 9b). This makes TF-10, TF-11, TF-12 and TF-13 tephra among the most relevant markers in the central Mediterranean region for synchronizing archives of different terrestrial and marine realms and exploring in detail the spatial and temporal variability and the different expression of the paleoclimatic and paleoenviromental processes spanning the MIS 5 interval (e.g. Regattieri et al., 2014; Zanchetta et al., 2016).

TF-17. The major and trace element composition of the glass from tephra TF-17, here dated at 158.8 ± 3.0 ka (Fig. 5), displays a wide compositional spectrum ranging from phonotephrite to phonolite (Figs. 8d and 9c). This notable variability matches that of the tephra CF-V5, found in the MIS 6 sediments of the nearby Campo Felice Basin (Giraudi et al., 2011; Giraudi and Giaccio, 2015), and of the layer OH-DP-0624/ OT0701-7 from Lake Ohrid succession (Leicher et al., 2016) (Fig. 8d). In both Campo Felice and Lake Ohrid successions the TF-17 equivalent occur just below the tephra correlated to the Vico B eruption (CF-V4 and OH-DP-0617, respectively; Giraudi et al., 2011; Giraudi and Giaccio, 2015; Leicher et al., 2016) dated at 157 ± 3 ka (Laurenzi and Villa., 1987). Based on this chronological indication and its glass composition

CF-V5 was tentatively correlated to Pitigliano Tuff, from Vulsini volcanic field, dated to 158 ± 11 ka and 155 ± 11 ka (Giraudi and Giaccio, 2015; Leicher et al., 2016). However, TF-17 tephra is characterized by Sr and Nd isotope ratios of ~0.70699 and ~0.51251, respectively (Tab. 1), i.e., similar to those featuring the volcanic rocks from the Neapolitan volcanoes and completely different from those of the Vulsini and generally of the Latium volcanoes (Fig. 4). OH-DP-0624 from Lake Ohrid has a similar Nd isotope composition (~0.51250) but a higher Sr isotope ratio (0.7105), which conceivably reflects alteration that has not been removed by leaching (e.g. D'Antonio et al., 2016). Therefore, based on Sr and Nd isotopic compositions of this tephra (Tab. 1; Fig. 4) the correlation with Pitigliano Tuff can be now ruled out and TF-17, as well as its equivalent OH-DP-0624 and CF-V5, can be confidently attributed to the Neapolitan volcanic area. This conclusion is definitively supported by the Cl versus CaO/FeO diagram, in which the TF-17 composition is well within the field of the Campi Flegrei rocks (Fig. 6). It is worthy of note that the Taurano Yellow Tuff, an ignimbrite deposit occurring on the eastern side of the Campanian Plain, was dated at 157.4 ± 2.0 ka (De Vivo et al., 2001); i.e., gechronologically indistinguishable from TF-17. However, the lack of glass compositional data for this ignimbrite currently prevent any attempt of comparison and definitive correlation.

Based on its peculiar compositional trend, Leicher et al. (2016) recognized a further equivalent layer of the tephra OH-DP-0624/CF-V5 occurring in MIS 6 sediments of the Adriatic Sea (tephra PRAD-3225 Bourne et al., 2015), previously attributed to Vico D eruption, and having a modelled age of ~139-121 ka. By extension, the TF-17 can be confidentially associated to all the aforementioned tephra CF-V5/OH-DP-0624/OT0701-7/PRAD-3225, which, in the light of its known distal occurrences, is candidate to become a potential wide dispersed marker for MIS 6 interval of the central Mediterranean area, and for which here is given the first direct $^{40}Ar/^{39}Ar$ age of 158.8 ± 3.0 ka.

5.2.3. Mt. Etna tephra (TF-3a and TF-3b)

TF-3a and TF-3b. The stratigraphic position in MIS 2 (Fig. 2) and the glass composition (Fig. 10a) of the two Etna layers generally matches that of the explosive eruptions related to Unit D, which encompasses the Biancavilla eruptive succession, dated at 18818-18550 cal BP, 18501-1805 cal BP, (unit Giarre D1a and D2a, Coltelli et al., 2000) and 17605-17065 cal BP (Biancavilla Ignimbrite, Siani et al., 2001) and which

generated the widespread Y-1 (e.g. Keller et al., 1978). A recent detailed study of the proximal Unit D/Biancavilla succession and of its potential distal counterparts (Albert et al., 2013) revealed that Y-1 actually represent only one of at least three tephra that can be potentially traced in distal settings and that are associated to different stages of the Unit D/Biancavilla eruptive succession spanning ~1.5 kyr.

Based on a comprehensive proximal and distal compositional datasets reported in this recent study, TF-3b is compositionally most similar to the layer TM-11 of Monticchio, Y1-LMZ of Lago di Mezzano (Fig. 10a) and the "Y-1" of Central Adriatic and Bannock Basin, which was attributed to a currently unidentified phase of the Unit D/Biancavilla eruptive succession and which differs significantly from the Ionian Sea Y-1 glasses (Fig. 10a) (Albert et al., 2013). The inferred age of this non-Ionian Sea like Y-1, based on a combination of ^{14}C dating and Monticchio chronology, is 18.4-17.6 ka (Albert et al., 2013).

The slightly younger layer TF-3a, although sharing with TF-3b a main benmoreitic composition (SiO_2 ~60 wt%), also contains trachytic glass shards (SiO_2 up to 63 wt%) that approach the composition of the Etna Acireale fall D1b and D2b, the latter correlated to the Ionian Sea Y-1 (Albert et al., 2013). We would thus be inclined to correlate TF-3a with the Acireale fall D1b and D2b and possibly with Ionian Sea Y-1. However, by considering the complexity of the Biancavilla eruption, the wide geochemical variability of the related eruptive units and the current uncertainties in correlating them to different distal Y-1-like tephra, we consider this as a tentative correlation, to be eventually reconsidered in the light of new data.

5.2.4. Colli Albani tephra (TF-4, TF-5, TF-8 and TF-9)

TF-4, TF-5, TF-8 and TF-9. The chronology and composition of these four foiditic tephra (Figs. 10b and 10c) constrain their correlation to the most recent activity of the Colli Albani caldera documented at the Albano maar by seven explosive events (Freda et al., 2006; Giaccio et al., 2007, 2009; De Benedetti et al., 2008; Sottili et al., 2009; Gaeta et al., 2011; Cross et al., 2014) clustered in two groups of eruptions dated between ~73-69 ka (Albano 1 to Albano 3) and ~40-36 ka (Albano 4 to Albano 7) (Freda et al., 2006; Giaccio et al., 2009; Marra et al., 2016).

Four out of seven eruptive units of the Albano suite (Albano 1, 3, 5 and 7) were generated by relatively high explosive, sub-Plinian events (Giaccio et al., 2007), making these units the most likely proximal counterparts of the four Fucino foiditic tephra TF-4, TF-5, T-8 and TF-9. Albano 7 in particular was considered the most

energetic and complex eruptive event (Giaccio et al., 2007). Indeed the thickness of TF-4 (up to 15 cm), which is the greater of this group of Albano tephra (Fig. 2), confirms both the higher magnitude of Albano 7 eruption and the prevailing NE-trending dispersion of its deposits inferred from isopleth and isopach maps of the mid-proximal area (Giaccio et al., 2007). The $^{40}Ar/^{39}Ar$ ages of the TF-4 and TF-5 yielded the ages of 45.0 ± 7.5 ka (2σ) and 39.4 ± 2.0 ka (2σ), respectively; i.e., statistically indistinguishable from the available $^{40}Ar/^{39}Ar$ dating of Albano 7 (37.0 ± 3.0 ka, 33.0 ± 4.0 ka, 35.9 ± 0.6 ka) and Albano 5 (41.0 ± 7.0) (Freda et al., 2006; Giaccio et al., 2009), thus ensuring our correlation. The $^{40}Ar/^{39}Ar$ ages of the proximal Albano 1 and Albano 3 units, respectively correlated to TF-9 and TF-8, range from 68.9 ± 0.2/69.4 ± 0.6 ka (Freda et al., 2006) to 72 ± 3 ka (Giaccio et al., 2009) and from 68.6 ± 1.1 ka (Freda et al., 2006) to 73.0 ± 3.0 ka (Giaccio et al., 2009), respectively.

So far, distal occurrences of Albano maar activity were limited to one or two layers of the most recent cluster of eruptions (i.e., 40-36 ka) as documented in central Italy (Giraudi et al., 2011; Giaccio et al., 2013) and Monticchio in southern Italy (Cross et al., 2014). Therefore, the Fucino tephra record provides the first evidence documenting, altogether and in stratigraphic order, the four most energetic explosive episodes of both early (i.e., Albano 1 and Albano 3 of ~73-69 ka) and late (i.e., Albano 5 and Albano 7 of ~40-36 ka) eruptive stages (Giaccio et al. 2007).

5.2.5. Ischia tephra (TF-7 and TF-21)

TF-7. Glasses from Ischia tephra are known for having a rather limited compositional variability (Tomlinson et al., 2014) making their individual recognition challenging. However, among the numerous Ischia tephra produced during the MIS 4-2 interval – e.g. as documented in the proximal setting (e.g. Brown et al., 2008) and by dozens of layers in the Monticchio record (Tomlinson et al., 2014) – the marine Y-7 tephra, correlated to the large caldera forming Monte Epomeo Green Tuff (MEGT), is the most widespread and thus the most probable correlative for TF-7. The MEGT has been recently dated to 56.5 ± 3.0 ka (Sbrana and Toccaceli, 2011), though details on data treatment, including use of a particular decay constant or nominal standard age, are currently not available. Indeed, the chemical composition of TF-7 glass matches both distal Y-7 layer and proximal MEGT (Fig. 10d). The proposed correlation is further supported by Sr isotopes of handpicked K-feldspars from TF-7 tephra (~0.70685), which is in the narrow range of the isotope

composition of the crystals from the proximal products of the MEGT (~0.706753 to ~0.706907; Brown et al., 2014). In addition, our $^{40}Ar/^{39}Ar$ dating of TF-7 at 56.1 ± 1.0 ka (2σ) is statistically indistinguishable from the age of the proximal MEGT, as well as from the age of the Monticchio equivalent tephra of the Y-7 marker (layer TM-19; Wulf et al., 2004; Tomlinson et al., 2014) dated by $^{40}Ar/^{39}Ar$ at 55 ± 2 ka (Watts et al., 1996), thus confirming the proposed correlation, though also in this case the decay constant and standard age used are not described. In this regard, since no analytical data are reported and discussed for both MEGT and TM-19 $^{40}Ar/^{39}Ar$ dating, our investigation provides the first, experimentally fully documented and precise $^{40}Ar/^{39}Ar$ age for the Y-7 tephra, regarded as an important marker of the central Mediterranean tephrostratigraphy (e.g. Tomlinson et al. 2014).

Thus the TF-7 represents a further finding which is added to the numerous occurrences of the Y-7 tephra and equivalent layers – e.g. TM-19 in Monticchio (Wulf et al., 2004); S-16 in San Gregorio Magno Basin, southern Italy (Munno and Petrosino, 2007); PRAD-1870 in core PRAD1-2, central Adriatic Sea (Bourne et al., 2010); and other successions as summarized in Tomlinson et al. (2014 and reference therein) – and which enlarges its northward aerial dispersal.

TF-21. This second Ischia tephra occurs at the base of the F1-F3 succession where lighter oxygen isotope compositions of the lake carbonates (Fig. 2) suggest that this stratigraphic interval corresponds to late MIS 7 interglacial/interstadial conditions. In Tyrrhenian Sea tephrostratigraphic records, at least two Ischia tephra are found in a comparable climatostratigraphic position; i.e., C-52 and C-54, astronomically dated at 185 ± 5 ka-189 ± 5 ka and 192 ± 5 ka (Paterne et al., 2008). The chemical composition of the glass from tephra TF-21 is closer to that of C-52 layer (Fig. 11a), but the correlation should be considered with caveats, because only average major element compositions are available for the C-52 and C-54 tephra layers. Furthermore these data were determined by SEM-EDS, which are not suitable for very precise comparisons with the WDS-EMPA data. For TF-21 we can therefore propose only a tentative correlation to C-52, and attributing to this tephra an age spanning between 185 ± 5 ka and 189 ± 5 ka.

5.2.6. Sabatini tephra (TF-14)

TF-14. This layer from the recent activity (i.e., 150-90 ka; Sottili et al., 2010) of the Sabatini volcanic district has been dated at 126.4 ± 1.0 (Fig. 5), which is fully consistent with its stratigraphic position slightly after the onset of the MIS 5 (Fig. 2). Between 150 ka and 89 ka several hydromagmatic centers were active in Sabatini volcanic district (Sottili et al., 2010). Unfortunately, to date, only very few pyroclastic units from this recent activity of this volcanic district have been characterized in terms of glass composition (e.g. Sottili et al., 2012), making the recognition of the potential TF-14 proximal counterpart difficult to identify. Sr and Nd isotopes suggest that TF-14 should be correlated to the Baccano Lower Unit (Sottili et al., submitted), dated at 131 ± 2 ka (Sottili et al. 2010), although both $^{40}Ar/^{39}Ar$ and major element composition (Fig. 11b) do not support the correlation. On the other hand, a very convincing chemical matching between TF-14 and the distal layer TM-36 of Monticchio record (Wulf et al., 2012) has been established (Fig. 11b). Encouragingly, tephra TM-36 also has a climatostratigraphic position similar to that of TF-14; i.e., slightly after the onset of the MIS 5 during the first drop in arboreal pollen percentage which marks the end of the early Eemian in Monticchio pollen record (Brauer et al., 2007; Wulf et al., 2012). This event could match the so-called middle-Eemian cooling event documented in central Italy speleothems (e.g. Regattieri et al., 2014) and possibly in Iberian Margin pollen (e.g. Sánchez Gõni et al., 1999) records.

According to the age model of Monticchio in Wulf et al. (2012), TM-36 would have an age of 123 ± 6.2 ka, whilst based on the age-depth data reported in Brauer et al. (2007), an age of ~124.4 ka should be expected at the depth of the tephra TM-36 (85.296 m; Wulf et al., 2012). These are younger than $^{40}Ar/^{39}Ar$ age of the TF-17, but still compatible within age uncertainty. Furthermore, according to the U/Th based age model of the Italian speleothem (e.g. Regattieri et al., 2014; Drysdale et al., 2005, 2009), the short middle-Eemian cooling event extends between ~126.6 to ~126.0 ka; i.e., in good agreement with the $^{40}Ar/^{39}Ar$ age of TF-14, thus highlighting a great consistence of the two U/Th and $^{40}Ar/^{39}Ar$ geochronological methods for this time period.

5.2.7. Vico tephra (TF-15 and TF-16)

TF-15 and TF-16. This set of Vico tephra occur in the middle of the MIS 6 glacial period, a few of meters above tephra TF-17, which is from the Neapolitan volcanic area and has a $^{40}Ar/^{39}Ar$ age of 158.8 ± 3.0 ka (Fig. 2). In the proximal setting at least three pyroclastic units are documented during the relevant time span

corresponding to the late and paroxysmal stage of the Period II as defined by Perini et al. (2004): Ronciglione Formation; Sutri Formation and Carbognano Formation, also known as Vico Ignimbrite B, Vico Ignimbrite C and Vico Ignimbrite D, dated at 157 ± 3 ka, 151 ± 1 ka and 138 ± 2 ka, respectively (Laurenzi and Villa, 1987). However, since also in this cases the decay constant and standard age used are not described, these ages have to be considered with caveats when comparing them with other $^{40}Ar/^{39}Ar$ ages.

As aforementioned, in the nearby Campo Felice succession the equivalent tephra of TF-17 – i.e., CF-V5 – was found just below the layer CF-V4 which in turn was correlated to the Vico B eruption (Giraudi and Giaccio., 2015). As matter of fact, the composition of the glass from tephra TF-16 matches both CF-V4 layer and its proximal counterpart represented by the Vico B pyroclastics (Fig. 11d), whilst the stratigraphically younger TF-15 layer has a glass composition very similar to Vico Ignimbrite C (Fig. 11c) (Palladino et al., 2014). We can thus conclude that TF-16 and TF-15 are the distal equivalents of Vico Ignimbrite B and Vico Ignimbrite C, respectively. The correlation of TF-16 to Vico B is further supported by the Sr and Nd isotope ratios of TF-16 (Tab. 1) that is very close to those of Vico B (e.g. 0.710521 ± 9-0.512139 ± 11 and 0.710490 ± 11-0.512132 ± 9; Perini et al., 2004) (Fig. 4).

Currently, in addition to the already mentioned CF-V4 in the nearby Campo Felice Basin, other convincing distal occurrences of TF-16/Vico B are limited to the Lake Ohrid succession (layer OH-DP-0617, Leicher et al., 2016). Indeed, layer OH-DP-0617 occurs just above the OH-DP-0624, which matches the tephra TF-17 (Fig. 9d), illustrating a consistent stratigraphic ordering between the Fucino and the Lake Ohrid tephra records. As far as TF-15/Vico C is concerned, in recent papers (Palladino et al., 2014; Bourne et al., 2015) a correlation has been proposed with the layer PRAD-3586 in core PRAD 1-2, equivalent to the layer 410/419 in core RF95-7, of the Adriatic Sea. However, this correlation is problematic on stratigraphic grounds given the position of PRAD-3586 with respect to other MIS 6 tephra identified in the record. Specifically, at Fucino TF-15/Vico C tephra occurs above TF-17 layer, yet the layer PRAD-3586, presumably associated to Vico C, is stratigraphically below PRAD-3225, which can be confidentially correlated to the TF-17 layer, i.e., indicating a reverse stratigraphic ordering. In any case, irrespective of the problematic and questionable identification of other distal equivalent of TF-15/Vico C tephra, the Fucino succession provides the first unambiguous evidence documenting the occurrence of the stratigraphically ordered distal equivalents of both Vico Ignimbrite B and Vico Ignimbrite C.

5.2.8. Latium-undefined volcanic source (TF-18/19, TF-20 and TF-22)

TF-18/19 and TF-20 occur close the underlying Ischia tephra TF-21 of ~185-190 ka, and thus chronologically are slightly younger than the former. TF-22 is instead at 17.3 m of depth of the core SPE core, which should correspond to ~112 m in composite section (Fig. 2). Taking into account the direct and indirect $^{40}Ar/^{39}Ar$ chronology available for both SPE core and composite section, and assuming mean sedimentation rates, a very rough age estimation of ~240-260 ka can be assessed in for this layer.

In terms of major element composition, TF-18/19, TF-20 and TF-22 tephra forms a homogenous group of phonolitic tephra featured by a relatively high alkali sum (14-15 wt%), a rather constant content of SiO_2 (57-58 wt%) (Fig. 3a) and a peculiar high content of F (up to >1 wt%), that is unmatched with respect other phonolitic-trachytic tephra from Fucino (see Supplementary Table S3). These features suggest a common volcanic source of the tephra, which however appear hardly identifiable.

According to the Cl vs CaO/FeO diagram these tephra should be sourced from the Roccamonfina volcano (Fig. 6). However, the Sr and Nd isotope compositions of the Roccamonfina post-caldera volcanic phase (~385-50 ka) range from ~0.7075-0.7067 and ~0.51227-0.51238, respectively, (Conticelli et al., 2009), i.e., significantly different from the ratios measured for the TF-20 tephra (0.710327 and 0.512118, respectively Tab. 1), that are typical of the Latium volcanism (Fig. 4). Actually, some large caldera-forming events from Vulsini volcanic district – such as Onano, Grotte di Castro, Sorano, Sovana, and Canino eruptions occurred between 160 ka and 250 ka (Palladino et al., 2010) – appear chronologically and volcanologically compatible with these tephra, but the available major element compositions of the glass from Vulsini units, though still incomplete (e.g. Palladino et al., 2014), may exclude such a volcanic source.

Finally, none of the tephra layers of core PRAD 1-2 from the Adriatic Sea (Bourne et al., 2015) is either chronologically or geochemically compatible with these tephra. Therefore, at present no reliable or even a tentative correlation with either proximal or distal counterparts can be proposed for these tephra.

6. Summary, perspectives and concluding remarks

This paper accounts the first integrated tephrochronological record of the uppermost ~10% (~84 m) of the ~900 m-thick Quaternary lacustrine succession of the Fucino Basin. The results of this study confirm and

substantially improve, on the basis of a wide and robust experimental dataset, the preliminary tephrochronological framework in Giaccio et al. (2015b) and definitively constrain the chronology of the investigated Fucino succession over the last ~190 kyr (Fig. 12). The WDS-EMPA major element composition of glass from 23 stratigraphically ordered tephra layers, along with LA-ICP-MS trace element analyses of selected layers, provided the geochemical fingerprinting needed for the reliable recognition of many layers (Fig. 12), some of which match important regional and extra-regional markers (e.g., NYT, Y-7, C-22, X-5 and X-6). Fucino thus stands as a new important node within the dense network of tephra correlations in the central Mediterranean area (Fig.13). The Sr and Nd isotope compositions of some selected tephra layers confirm the robustness of this kind of analysis for consistently circumscribing the volcanic source of distal tephra and possibly for recognizing individual eruptive units. Furthermore, for the first time the Sr and Nd isotopic compositions of some of the most important stratigraphic markers in the central Mediterranean area (Y-7, X-5 and X-6) have been determined, thus providing the first isotopic fingerprinting which confirms their volcanic sources from Ischia (Y-7) and the Neapolitan volcanic area, likely Campi Flegrei, (X-5 and X-6). In this contribution we have also proposed a new more expeditious method for identifying the source of trachyte-phonolite and tephri-phonolite tephra – that are the most common compositions of the pyroclastic products from Campanian and Latium volcanoes – via a key diagram based on Cl wt% content and CaO/FeO ratio in the volcanic glasses. Finally, we provided new $^{40}Ar/^{39}Ar$ ages for five tephra layers, including a new analytically well-supported and more precise $^{40}Ar/^{39}Ar$ age for the widespread Y-7 tephra (56.1 ± 1.0 ka), and the first $^{40}Ar/^{39}Ar$ ages for the tephra TF-14 (126.4 ± 1.0 ka), from the Sabatini volcanic district, and for tephra TF-17 (158.8 ± 3.0 ka), from the Neapolitan volcanic area. These two latter tephra have been also traced in other successions at hundreds of km from the respective volcanic sources (i.e., TF-14 in Lake Monticchio and TF-17 in Adriatic Sea and Lake Ohrid) and thus have the potential to become important markers for the Mediterranean MIS 5 and MIS 6 time periods (Fig. 13).

Although the available direct and indirect dating of at least 19 out of 23 layers would have allowed the construction of a relatively robust, statistically-based age model, here it is deliberately avoided because a detailed discussion of the chronology of the Fucino succession will be addressed elsewhere, in the more suitable framework of a paper specifically focused on geochronology and high-resolution palaeoclimate and palaeoenvironmental proxies, the acquisition of which, alongside new $^{40}Ar/^{39}Ar$ dating, are currently in

progress. To this regard, we note that the $^{40}Ar/^{39}Ar$ ages discussed herein are based on calibrations (Nomade et al., 2005) and the decay constants (Steiger and Jäger, 1977) that are subject to possible, even if slight, changes (e.g. Niespolo et al., 2016). Nevertheless, it is remarkable noting how – by means of a simple linear interpolation between the Fucino tephra ages and the depth proxy series – the variability of the lake primary productivity and temperature, reflected by the Ca content from the Fucino sediments (Giaccio et al., 2015b), is strictly consistent with the chronology and the general trends of the main and millennial-scale climatic fluctuations over the last 190 kyr as documented by reference Mediterranean records (e.g. Martrat et al., 2004) (Fig. 12). The well documented suitability of the Fucino tephra to provide a robust independent chronology (based on both direct and indirect $^{40}Ar/^{39}Ar$ dating) and the high climatic sensitivity of the Fucino sediments, along with the exceptionally long and continuous sedimentary history of the basin, make the Fucino succession ideally suited for getting a radioisotopic-based time-scale for a Quaternary event stratigraphy extending back to at least 1.5 Ma. Through direct synchronization (tephra correlations) and paleoclimatic alignments, the Fucino chronology can be arguably applied to records on extra-regional to semi-global scales (e.g. Zanchetta et al., 2016), thus becoming a key reference template for understanding the Quaternary paleoclimatology and geochronology of a wide planet area, which extends well beyond the central Mediterranean region.

Acknowledgments

BG thanks Emanuela Falcucci, Fabrizio Galadini, Stefano Gori and Giancarlo Scardia for having contributed to the stratigraphic logging of the cores SP and SPE carried out on field in 2012, and Marcello Serracino for his valuable assistance during EMP analyses at Istituto di Geologia Ambientale e Geoingegneria – CNR, Roma. EMN and PRR thank the Ann and Gordon Getty Foundation and NSF grant BCS-1322017 for facilities support. BW thanks German Research Foundation, CRC 806 “Our way to Europe” for the partial financial support. The manuscript benefited from useful comments from two anonymous reviewers.

References

Albert, P. G., 2012. Volcanic glass geochemistry of Italian proximal deposits linked to distal archives in the central Mediterranean region. PhD Thesis, Royal Holloway University of London.

Albert, P.G., Tomlinson, E.L., Lane, C.S., Wulf, S., Smith, V.C., Coltelli, M., Keller, J., Lo Castro, D., Manning, C.J., Muller, W., Menzies, M.A., 2013. Late glacial explosive activity on Mount Etna: implications for proximal-distal tephra correlations and the synchronization of Mediterranean archives. J. Volcanol. Geotherm. Res. 265, 9–26.

Andronico, D., 1997. La Stratigrafia dei prodotti dell'eruzione di Lagno Amendolare (Phlegrean Fields, Napoli). Atti della Società Toscana di Scienze Naturali residente in Pisa. Memorie. Serie A 104, 165–178.

Blockley, S.P.E., Bronk Ramsey, C., Pyle, D.M., 2008. Improved age modelling and high-precision age estimates of late Quaternary tephras, for accurate palaeoclimate reconstruction. J. Volcanol. Geotherm. Res. 177, 251–262.

Boari, E., Avanzinelli, R., Melluso, L., Giordano, G., Mattei, M., De Benedetti, A.A., Morra, V., Conticelli, S., 2009a. Isotope geochemistry (Sr–Nd–Pb) and petrogenesis of leucitebearing volcanic rocks from Colli Albani volcano, Roman Magmatic Province, Central Italy: inferences on volcano evolution and magma genesis. Bulletin of Volcanology 71, 977–1005.

Boari, E, Tommasini, S., Laurenzi, MA., Conticelli S. 2009b. Transition from Ultrapotassic Kamafugitic to Sub-alkaline Magmas: Sr, Nd, and Pb Isotope, Trace Element and 40Ar-39Ar Age Data from the Middle Latin Valley Volcanic Field, Roman Magmatic Province, Central Italy. Journal of Petrology, 50, 1327–1357. doi:10.1093/petrology/egp003.

Bourne, A., Lowe, J.J., Trincardi, F., Asioli, A., Blockley, S.P.E., Wulf, S., Matthews, I.P., Piva, A., Vigliotti, L. 2010. Distal tephra record for the last ca. 105,000 years from core PRAD 1-2 in the central Adriatic Sea: implications for marine tephrostratigraphy. Quaternary Science Reviews 29, 3079–3094.

Bourne, A.J., Albert, P.G., Matthews, I.P., Trincardi, F., Wulf, S., Asioli, A., Blockley, S.P., Keller, J., Lowe J.J. 2015. Tephrochronology of core PRAD 1–2 in the Adriatic Sea: insights into Italian explosive volcanism for the period 200–80 ka. Quaternary Science Reviews 16, 28–43.

Brauer, A., Allen, J.R.M., Mingram, J., Dulski, P.,Wulf, S., Huntley, B., 2007. Evidence for the last interglacial chronology and environmental change from Southern Europe. Proceedings of the National Academy of Sciences of the United States of America 104, 450–455.

Brauer, A., Hajdas, I., Blockley, S.P., Ramsey, C.B., Christl, M., Ivy-Ochs, S., Moseley, G.E., Nowaczyk, N.N., Rasmussen, S.O., Roberts, H.M., 2014. The importance of independent chronology in integrating records of past climate change for the 60–8 ka INTIMATE time interval. Quaternary Science Reviews 106, 47–66.

Bronk Ramsey, C., Albert P., Blockley, S., Hardiman, M., Lane, C., Macleod, A., Matthews, I.P., Muscheler, R., Palmer, A., Staff, R.A., 2014. Integrating timescales with time-transfer functions: a practical approach for an INTIMATE database. Quaternary Science Reviews 106, 67–80.

Bronk Ramsey, C., Albert, P.G., Blockley, S.P.E., Hardiman, M., Housley, R.A., Lane, C.S., Lee, S., Matthews, I.P., Smith, V.C., Lowe, J., 2015. The chronology of the RESET tephra lattice. Quat. Sci. Rev. 118, 18–32.

Brown, R.J., Civetta, L., Arienzo, I., D'Antonio, M., Moretti, R., Orsi, G., Tomlinson, E.L., Albert, P.G., Menzies, M.A., 2014. Geochemical and isotopic insights into the assembly, evolution and disruption of a magmatic plumbing system before and after a cataclysmic caldera-collapse eruption at Ischia volcano (Italy). Contrib. Mineral. Petrol. 168, 1035.

Capotondi, L., Girone, A., Lirer, F., Bergami, C., Verducci, M., Vallefuoco, M., Afferri, A., Ferraro, L., Pelosi, N., De Lange, G.J., 2015. Central Mediterranean Mid-Pleistocene palaeoclimatic variability and its association with global climate, Palaeogeography, Palaeoclimatology, Palaeoecology, doi: 10.1016/j.palaeo.2015.11.009.

Cavinato, G.P., Carusi, C., Dall'Asta, M., Miccadei, E., Piacentini, T., 2002. Sedimentary and tectonic evolution of Plio–Pleistocene alluvial and lacustrine deposits of Fucino Basin (central Italy). Sedimentary Geology 148, 29–59.

Civetta, L., Orsi, G., Pappalardo, L., Fisher, R. V., Heiken, G., Ort, M. 1997. Geochemical zoning, mingling, eruptive dynamics and depositional processes; the Campanian Ignimbrite, Campi Flegrei caldera, Italy. Journal of Volcanology and Geothermal Research75, 183–19.

Coltelli, M., Del Carlo, P., Vezzoli, L., 2000. Stratigraphic constraints for explosive activity in the past 100 ka at Etna Volcano, Italy. International Journal of Earth Sciences 89, 665–667.

Conticelli, S., Francalanci, L., Manetti, P., Cioni, R., Sbrana, A., 1997. Petrology and geochemistry of the ultrapotassic rocks from the Sabatini Volcanic District, central Italy: the role of evolutionary processes in the genesis of variably enriched alkaline magmas. Journal of Volcanology and Geothermal Research 75, 107–136.

Conticelli, S., Marchionni, S., Rosa, D., Giordano, G., Boari, E., Avanzinelli, R., 2009. Shoshonite and sub-alkaline magmas from an ultrapotassic volcano: Sr–Nd–Pb isotope data on the Roccamonfina volcanic rocks, Roman Magmatic Province, Southern Italy. Contrib. Mineral. Petrol. 157, 41–63, doi: 10.1007/s00410-008-0319-8.

Corsaro, R.A., Di Renzo, V., Distefano, S., Miraglia, L., Civetta L., 2013. Relationship between magmatic processes in the plumbing system of Mt. Etna and the dynamics of the eastern flank: inferences from the petrologic study of the products erupted from 1995 to 2005. Journal of Volcanology and Geothermal Research 251, 75–89.

Cross, J.K., Tomlinson, E.L., Giordano, G., Smith, V.C., De Benedetti, A.A., Roberge, J., Manning, C., Wulf, S., Menzies, M.A., 2014. High level triggers for explosive mafic volcanism: Albano Maar, Italy. Lithos 190–191, 137–153.

D'Antonio M., Arienzo I., Mariconte R., Mazzeo F.C., Perugini D., Petrelli M., Civetta L., Corselli C., Orsi G., Principato M.S., 2016 . Combined Sr-Nd isotopic and geochemical fingerprinting as a tool to identify tephra layers: application to deep-sea cores from Eastern Mediterranean Sea. Chemical Geology 443, 121–136, doi: 10.1016/j.chemgeo.2016.09.022.

D'Antonio, M., Tonarini, S., Arienzo, I., Civetta, L., Di Renzo, V., 2007. Components and processes in the magma genesis of the Phlegrean Volcanic District, southern Italy. In: Beccaluva, L., Bianchini, G., Wilson, M. (Eds.), Cenozoic volcanism in the Mediterranean area. Geol. Soc. Am. Spec. Pap. 418, pp. 203–220. http://dx.doi.org/10.1130/2007. 2418(10) (Geol. Soc. Am., Boulder, CO,).

D'Antonio, M., Tonarini, S., Arienzo, I., Civetta, L., Dallai, L., Moretti, R., Orsi, G., Andria, M., Trecalli, A., 2013. Mantle and crustal processes in the magmatism of the Campania region: inferences from

mineralogy, geochemistry, and Sr-Nd-O isotopes of young hybrid volcanics of the Ischia island (South Italy). Contributions to Mineralogy and Petrology, 165, 1173–1194, doi: 10.1007/s00410-013-0853-x.

De Benedetti, A.A., Funiciello, R., Giordano, G., Diano, G., Caprilli, E., Paterne, M., 2008. Volcanology, history and myths of the Lake Albano maar (Colli Albani volcano, Italy). J. Volcanol. Geotherm. Res. 176, 387–406.

Deino, A., Potts, R., 1990. Single-Crystal $^{40}Ar/^{39}Ar$ Dating of the Olorgesailie Formation, Southern Kenya Rift. Journal of Geophysical Research 95, B6, 8453–8470.

Del Bello, E. Mollo S., Scarlato, P., von Quadt, A., Forni, F., Bachmann, O., 2014. New petrological constraints on the last eruptive phase of the Sabatini Volcanic District (central Italy): Clues from mineralogy, geochemistry and Sr–Nd isotopes. Lithos 205, 28–38.

Deino, A. L., Orsi, G., Piochi, M., de Vita, S., 2004. The age of the Neapolitan Yellow Tuff caldera-forming eruption (Campi Flegrei caldera, Italy) assessed by $^{40}Ar/^{39}Ar$ dating method. J. Volcanol. Geoth. Res. 133, 157–170.

Di Renzo, V., Arienzo, I., Civetta, L., D'Antonio, M., Tonarini, S., Di Vito, M.A., Orsi, G., 2011. The magmatic feeding system of the Campi Flegrei caldera: architecture and temporal evolution. Chem. Geol. 281, 227–241.

De Vivo, B., Rolandi, G., Gans, P.B., Calvert, A., Bohrson, W.A., Spera, F.J., Belkin, H.E., 2001. New constraints on the pyroclastic eruptive history of the Campanian Volcanic Plain (Italy). Contrib. Mineral. Petrol. 73, 47–65.

Di Renzo, V., Di Vito, M.A., Arienzo, I., Carandente, A., Civetta, L., D'antonio, M., Giordano, F., Orsi, G., Tonarini, S., 2007. Magmatic history of Somma-Vesuvius on the basis of new geochemical and isotopic data from a deep borehole (Camaldoli della Torre). Journal of Petrology 48, 753–784.

Di Vito, M.A., Isaia, R., Orsi, G., Southon, J., de Vita, S., D'Antonio, M., Pappalardo, L., Piochi, M., 1999. Volcanism and deformation since 12,000 years at the Campi Flegrei caldera (Italy). Journal of Volcanology and Geothermal Research 91, 221-246.

Donato, P., Albert, P.G., Crocitti, M., De Rosa, R., Menzies, M.A. 2016. Tephra layers along the southern Tyrrhenian coast of Italy: Links to the X-5 & X-6 using volcanic glass geochemistry", Journal of Volcanology and Geothermal Research 317, 30–41.

Drysdale R.N, Zanchetta G., Hellstrom J.C, Fallick, A.E., Zhao, J.X., 2005. Stalagmite evidence for the onset of the Last Interglacial in southern Europe at 129 ± 1 ka. Geophysical Research Letters 32, 1–4.

Drysdale, R.N., Zanchetta, G., Hellstrom, J.C., Fallick, A.E., Sanchez-Goni, M.F., Couchoud, I., McDonald, J., Maas, R., Lohmann, G., Isola, I., 2009. Evidence for obliquity forcing of glacial termination II. Science 325, 1527–1531.

Esposito, R., Bodnar, R. J., Danyushevsky, L. V., De Vivo, B., Fedele, L., Hunter, J., Lima A., Shimizu, N. (2011). Volatile evolution of magma associated with the Solchiaro eruption in the Phlegrean Volcanic District (Italy). Journal of Petrology 52, 2431–2460.

Fabbrizio, A., Carroll, M.R., 2008. Experimental constraints on the differentiation process and pre-eruptive conditions in the magmatic system of Phlegraean Fields (Naples, Italy). Journal of Volcanology and Geothermal Research 171, 88–102.

Fowler, S. J., Spera, F. J., Bohrson, W. A., Belkin, H. E., De Vivo, B., 2007. Phase equilibria constraints on the chemical and physical evolution of the Campanian Ignimbrite. Journal of Petrology 48, 459–493.

Freda, C., Gaeta, M., Karner, D.B., Marra, F., Renne, P.R., Taddeucci, J., Scarlato, P., Christensen, J.N., Dallai, L., 2006. Eruptive history and petrologic evolution of the Albano multiple maar (Alban Hills, Central Italy). Bulletin of Volcanology 68, 567–591.

Gaeta, M., Di Rocco, T., Freda, C., 2009. Carbonate assimilation in open magmatic systems: the role of melt-bearing skarns and cumulate-forming processes. Journal of Petrology 50, 361–385.

Gaeta, M., Freda, C., Christensen, J. N., Dallai, L., Marra, F., Karner, D. B., Scarlato, P., 2006. Time-dependent geochemistry of clinopyroxene from the Alban Hills (Central Italy): clues to the source and evolution of ultrapotassic magmas. Lithos 86, 330–346.

Gaeta, M., Freda, C., Marra, F., Arienzo, I., Gozzi, F., Jicha, B., Di Rocco, T., 2016. Paleozoic metasomatism at the origin of Mediterranean ultrapotassic magmas: Constraints from time-dependent geochemistry of Colli Albani volcanic products (Central Italy). Lithos 244, 151–164.

Gaeta, M., Freda, C., Marra, F., di Rocco, T., Gozzi, F., Arienzo, I., Giaccio, B., Scarlato, P., 2011. Petrology of the most recent ultrapotassic magmas from the Roman Province (Central Italy). Lithos 127, 298–308.

Galadini, F., Galli, P. 2000. Active tectonics in the central Apennines (Italy) – input data for seismic hazard assessment, Natural Hazards 22, 225–270.

Galli, P., Messina, P., Giaccio, B., Peronace, E., Quadrio, B., 2012. Early Pleistocene to Late Holocene activity of the Magnola Fault (Fucino Fault System, central Italy). Bollettino di Geofisica Teorica ed Applicata, 53, 435–458.

Galli, P., Giaccio, B., Messina, P., Peronace, E., 2016a. Three magnitude 7 earthquakes on a single fault in central Italy in 1400 years evidenced by new palaeoseismic results. Terra Nova 28, 146–154.

Galli, P., Giaccio, B., Messina, P., Peronace, E., Amato, V., Naso, J., Nomade, S., Pereira, A., Piscitelli, S., Bellanova, J., Billi, A., Blamart, D., Galderisi, A., Giocoli, A., Stabile, T., Thil, F., 2016b. Middle to Late Pleistocene activity of the northern Matese fault system (southern Apennines, Italy). Tectonophysics, submitted.

Galli, P., Giaccio, B., Peronace, E., Messina, P., 2015. Holocene paleoearthquakes and early-late pleistocene slip-rate on the Sulmona Fault (Central Apeninnes, Italy). Bull. Seism. Soc. Am. 105, 1–13.

Giaccio, B., Arienzo, I., Sottili, G., Castorina, F., Gaeta, M., Nomade, S., Galli, P., Messina, P., 2013a. Isotopic (Sr-Nd) and major element fingerprinting of distal tephras: an application to the Middle-Late Pleistocene markers from the Colli Albani volcano, central Italy. Quat. Sci. Rev. 67, 190–206.

Giaccio, B., Castorina, F., Nomade, S., Scardia, G., Voltaggio, M., Sagnotti, L., 2013b. Revised Chronology of the Sulmona Lacustrine Succession, Central Italy. Journal of Quaternary Science 28, 545–551.

Giaccio, B., Marra, F., Hajdas, I., Karner, D. B., Renne, P.R., Sposato, A., 2009. $^{40}Ar/^{39}Ar$ and ^{14}C geochronology of the Albano maar deposits: Implications for defining the age and eruptive style of the most recent explosive activity at Colli Albani Volcanic District, Central Italy. Journal of Volcanology and Geothermal Research 185, 203–213.

Giaccio, B., Nomade, S., Wulf, S., Isaia, R., Sottili, G., Cavuoto, G., Galli, P., Messina, P., Sposato, A., Sulpizio, R., Zanchetta, G., 2012.The late MIS 5 Mediterranean tephra markers: A reappraisal from peninsular Italy terrestrial records. Quaternary Science Reviews 56, 31–45.

Giaccio, B., Regattieri, E., Zanchetta, G., Nomade, S., Renne, P.R., Sprain, C.J., Drysdale, R.N., Tzedakis, P.C., Messina, P., Scardia, G., Sposato, A., Bassinot, F., 2015a. Duration and dynamics of the best orbital analogue to the present interglacial. Geology 43, 603–606.

Giaccio, B., Regattieri, E., Zanchetta, G., Wagner, B., Galli, P., Mannella, G., Niespolo, E., Peronace, E., Renne, P., Nomade, S., Cavinato, G.P., Messina, P., Sposato, A., Boschi, C., Florindo, F., Marra, F., Sadori, L., 2015b. A key continental archive for the last 2 Ma of climatic history in central Mediterranean area: a preliminary report on the Fucino deep-drilling project, central Italy. Scientific Drilling 3, 1–7, DOI: 10.5194/sd-3-1-2015.

Giaccio, B., Sposato, A., Gaeta, M., Marra, F., Palladino, D. M., Taddeucci, J., Barbieri, M., Messina, P., Rolfo, M.F. 2007. Mid-distal occurrences of the Albano Maar pyroclastic deposits and their relevance for reassessing the eruptive scenarios of the most recent activity at the Colli Albani Volcanic District, Central Italy. Quaternary International 171-172, 160–178.

Giaccio, B., Galli, P., Peronace, E., Arienzo, I., Nomade, S., Cavinato, G.P., Mancini, M., Messina, P., Sottili, G., 2014. A 560–440 ka tephra record from the Mercure Basin, southern Italy: volcanological and tephrostratigraphic implications. Journal of Quaternary Science 29, 232–248.

Giraudi, C., Bodrato, G., Lucchi, M. R., Cipriani, N., Villa, I. M., Giaccio, B., and Zuppi, G. M.: Middle and late Pleistocene glaciations in the Campo Felice Basin (central Apennines, Italy), Quaternary Research 75, 219–230,.

Giraudi, C., Giaccio, B., 2015. The Middle Pleistocene glaciations on the Apennines (Italy): New chronological data and considerations about the preservation of the glacial deposits. Geological Society, London, Special Publications, 433 (5), doi:10.1144/SP433.1.

Gozzi, F., Gaeta, M., Freda, C., Mollo, S., Di Rocco, T., Marra, F., Dallai, L., Pack, A., 2014. Primary magmatic calcite reveals origin from crustal carbonate. Lithos 190, 191–203.

Granati, S. F., Perinelli, C., Gaeta, M., Freda, C., D'Antonio, M. (2014). Experimental constraints on phase relations in a multilevel magmatic system: the Phlegrean Volcanic District (South Italy) case study. Rendiconti online della Società Geologica Italiana, 31(Suppl. n. 1), 495-495.

Insinga, D.D., Tamburrino, S., Lirer, F., Vezzoli, L., Barra, M., De Lange, G.J., Tiepolo, M., Vallefuoco, M., Mazzola, S., Sprovieri, M., 2014. Tephrochronology of the astronomically-tuned KC01B deep-sea core, Ionian Sea: Insights into the explosive activity of the Central Mediterranean area during the last 200ka. Quaternary Science Reviews 85, 63–84.

Iorio, M., Liddicoat, J., Budillon, F., Incoronato, A., Coe, R.S., Insinga, D.D., Cassata, W.S., Lubritto, C., Angelino, A., Tamburrino, S., 2014. Combined palaeomagnetic secular variation and petrophysical records to time constrain geological and hazardous events: an example from the eastern Tyrrhenian Sea over the last 120 ka. Global and Planetary Changes 113, 91–109.

Jolis, E.M., Troll, V., Harris, C., Freda, C., Gaeta, M., Orsi, G., Siebe, C., 2015. Skarn xenolith record crustal CO2 liberation during Pompeii and Pollena eruptions, Somma-Vesuvius volcanic system. Chemical Geology 415, 17–36.

Kamenetsky, V.S., Mitchell, R. H., Maas, R., Giuliani, A., Gaboury, D., Zhitova, L., 2015. Chlorine in mantle-derived carbonatite melts revealed by halite in the St.-Honoré intrusion (Québec, Canada). Geology, 43, 687–690.

Karner, D.B., Juvigne´, E., Brancaccio, L., Cinque, A., Russo Ermolli, E., Santangelo, N., Bernasconi, S., Lirer, L., 1999. A potential early middle Pleistocene tephrostratotype for the Mediterranean Basin: the Vallo di Diano, Campania, Italy. Global and Planetary Change 21, 1–15.

Keller, J., Ryan, W.B.F., Ninkovich, D., 1978. Explosive volcanic activity in the Mediterranean over the past 200,000 yrs as recorded in deep-sea sediments. Geol. Soc. America Bull. 89, 591–604.

Lane, C.S., Andri_c, M., Cullen, V.L., Blockley, S.P.E., 2011. The occurrence of distal Icelandic and Italian tephra in the Lateglacial of Lake Bled, Slovenia. Quaternary Science Reviews. 30, 1013–1018.

Lane, C.S., Brauer, A., Martín-Puertas, C., Blockley, S.P.E., Smith, V.C., Tomlinson, E.L., 2015. The Late Quaternary tephrostratigraphy of annually laminated sediments from Meerfelder Maar, Germany. Quaternary Science Reviews 122, 192–206.

Laurenzi, M.A., Villa, I.M., 1987. $^{40}Ar/^{39}Ar$ chronostratigraphy of Vico ignimbrites. Periodico di Mineralogia 56, 285–293.

Le Maitre, R.W., 2002. Igneous Rocks: A Classification and Glossary of Terms: Recommendations of the International Union of Geological Sciences, Subcommission on the Systematics of Igneous. Cambridge University Press, Rocks (236 pp.).

Lee, J.Y., Marti, K., Severinghaus, J.P., Kawamura, K., Yoo, H.-S., Lee, J.B., Kim, J.S., 2006. A redetermination of the isotopic abundances of atmospheric Ar. Geochimica et Cosmochimica Acta 70, 4507–4512.

Leicher, N., Zanchetta, G., Sulpizio, R., Giaccio, B., Wagner, B., Nomade, S., Francke, A., and Del Carlo, P.: First tephrostratigraphic results of the DEEP site record from Lake Ohrid (Macedonia and Albania). Biogeosciences 13, 2151–2178, doi:10.5194/bg-13-2151-2016.

Lowe, D.J., 2011. Tephrochronology and its application: A review. Quaternary Geochronology 6, 107–153.

Lowe, J., Barton, N., Blockley, S., Ramsey, C.B., Cullen, V.L., Davies, W., Gamble, C., Grant, K., Hardiman, M., Housley, R., Lane, C.S., Lee, S., Lewis, M., MacLeod, A., Menzies, M., Müller, W., Pollard, M., Price, C., Roberts, A.P., Rohling, E.J., Satow, C., Smith, V.C., Stringer, C.B., Tomlinson, E.L., White, D., Albert, P., Arienzo, I., Barker, G., Borić, D., Carandente, A., Civetta, L., Ferrier, C., Guadelli, J.-., Karkanas, P., Koumouzelis, M., Müller, U.C., Orsi, G., Pross, J., Rosi, M., Shalamanov-Korobar, L., Sirakov, N., Tzedakis, P.C, 2012. Volcanic ash layers illuminate the resilience of Neanderthals and early modern humans to natural hazards. Proceedings of the National Academy of Sciences of the United States of America 109, 13532–13537.

Ludwig, K.R., 2001. Isoplot 3.0da Geochronological Toolkit for Microsoft Excel: Special Publication No. 4. Berkeley Geochronology Center, Berkeley, Calif, 71 pp.

Maiorano, P., Tarantino, F., Marino, M., De Lange, G.J., 2013. Paleoenvironmental conditions at Core KC01B (Ionian Sea) through MIS 13–9: evidence from calcareous nannofossil assemblages. Quaternary International 288, 97–111.

Marchini, G., Zanchetta, G., Santacroce, R., Vigliotti, L., Capotondi, L., Sulpizio, R., 2014 Tephrostratigraphy of marine core AD91-17 (Adriatic Sea) Revised, Alpine and Mediterranean Quaternary, 27, 77–84.

Marra, F., Gaeta, M., Giaccio, B., Jicha, B. R., Palladino, D. M., Polcari, M., Sottilli, G., Taddeucci, J., Florindo, F., Stramondo, S., 2016. Assessing the volcanic hazard for Rome: $^{40}Ar/^{39}Ar$ and In-SAR constraints on the most recent eruptive activity and present-day uplift at Colli Albani Volcanic District. Geophysical Research Letters 43, doi: 10.1002/2016GL069518.

Marra, F., Sottili, G., Gaeta, M., Giaccio, B., Jicha, B., Masotta, M., Palladino, D.M., Deocampo, D.M., 2014. Major explosive activity in the Monti Sabatini Volcanic District (central Italy) over the 800-390 ka interval: Geochronological-geochemical overview and tephrostratigraphic implications. Quaternary Science Reviews 94, 74–101.

Marra, F., Karner, D.B., Freda, C., Gaeta, M., Renne, P.R., 2009. Large mafic erup-tions at the Alban Hills Volcanic District (Central Italy): chronostratigraphy, petrography and eruptive behavior. J. Volcanol. Geotherm. Res.179, 217–232.

Martrat, B., Grimalt, J.O., Lopez-Martinez, C., Cacho, I., Sierro, F.J., Flores, J.A., Zahn, R., Canals, M., Curtis, J.A., Hodell, D.A., 2004. Abrupt temperature changes in the western Mediterranean over the past 250,000 years. Science 306, 1762–1765.

Masotta, M., Mollo, S., Gaeta, M., Freda, C., 2016. Melt extraction in mush zones: The case of crystal-rich enclaves at the Sabatini Volcanic District (central Italy). Lithos 248, 288–292.

Mathez, E. A., Webster, J. D., 2005. Partitioning behavior of chlorine and fluorine in the system apatite-silicate melt-fluid. Geochimica et Cosmochimica Acta 69, 1275-1286.

Munno, R., Petrosino, P., 2007. The late quaternary tephrostratigraphical record of the San Gregorio Magno basin (southern italy). Journal of Quaternary Science 22, 247–66.

Niespolo, E.M., Rutte, D., Deino, A.L., Renne, P.R., 2016. Intercalibration and age of the Alder Creek sanidine $^{40}Ar/^{39}Ar$ standard. Quaternary Geochronology, doi:10.1016/j.quageo.2016.09.004.

Nomade, S., Renne, P.R., Vogel, N., Deino, A.L., Sharp, W.D., Becker, T.A., Jaouni, A.R., Mundil, R., 2005. Alder Creek sanidine (ACs-2): A Quaternary Ar-40/Ar-39 dating standard tied to the Cobb Mountain geomagnetic event. Chemical Geology 218, 315–338.

Orsi, G., de Vita, S., Di Vito, M.A., 1996. The restless, resurgent Campi Flegrei nested caldera (Italy): constraints on its evolution and configuration. J. Volcanol. Geotherm. Res. 74, 179–214.

Pabst, S., Wörner, G., Civetta, L., Tesoro, R., 2008. Magma chamber evolution prior to the Campanian Ignimbrite and Neapolitan Yellow Tuff eruptions (Campi Flegrei, Italy). Bulletin of Volcanology 70, 961–976.

Palladino, D. M., Gaeta, M., Giaccio, B., Sottili, G., 2014. On the anatomy of magma chamber and caldera collapse: the example of trachy-phonolitic explosive eruptions of the Roman Province (central Italy), J. Volcanol. Geotherm. Res. 281, 12–26.

Palladino, D.M., Simei, S., Sottili, G., Trigila, R., 2010. Integrated approach for the reconstruction of stratigraphy and geology of Quaternary volcanic terrains: an application to the Vulsini Volcanoes

(central Italy). In: Groppelli, G., Viereck, L. (Eds.), Stratigraphy and geology in volcanic areas. Geological Society of America Special Paper 464, p. 63–84, doi: 10.1130/2010.2464(04).

Palladino, D., Gaeta, M., Marra, F., 2001. A large K-foiditic hydromagmatic eruption from the early activity of the Alban Hills Volcanic District, Italy. Bulletin of Volcanology 63, 345–359.

Pappalardo, L., Civetta, L., D'Antonio, M., Deino, A., Di Vito, M.A., Orsi, G., Carandente, A., de Vita, S., Isaia, R., Piochi, M., 1999. Chemical and Sr- isotopic evolution of the Phlegrean magmatic system before the Campanian Ignimbrite and the Neapolitan Yellow Tuff eruptions. J. Volcanol. Geotherm. Res. 91, 141–166.

Paterne, M., Guichard, F., Duplessy, J.C., Siani, G., Sulpizio, R., Labeyrie, J., 2008. A 90,000–200,000 years marine tephra record of Italian volcanic activity in the Central Mediterranean Sea. Journal of Volcanology and Geothermal Research 177, 187–196.

Peccerillo, A., 2005. Plio-Quaternary Volcanism in Italy. Springer-Verlag: Berlin, Heidelberg.

Pereira A., Nomade S., Voinchet P., Bahain J-J, Falguères C., Garon H., Lefèvre D., Raynal J-P., Scao V., Piperno M (2015). The earliest securely dated hominid fossil in Italy: Evidences of Acheulian human occupations during glacial MIS 16 at Notarchirico (Venosa, Basilicata, Italy). Journal of Quaternary Sciences 30, 639–650.

Perini, G., Francalanci, L., Davidson, J.P., Conticelli, S., 2004. Evolution and genesis of magmas from Vico Volcano, Central Italy: multiple differentiation pathways and variable parental magmas. J. Petrol. 45, 139–182.

Petrosino, P., Morabito, S., Jicha, B.R., Milia, A., Sprovieri, M., Tamburrino, S., 2016. Multidisciplinary tephrochronological correlation of marker events in the eastern Tyrrhenian Sea between 48 and 105 ka. Journal of Volcanology and Geothermal Research 31, 79–99, doi:10.1016/j.jvolgeores.2016.02.001.

Petrosino, P., Jicha, B., Mazzeo, F.C., Russo Ermolli, E.A., 2014. High resolution tephrochronological record of MIS 14-12 in the Southern Apennines (Acerno basin, Italy). J. Volcanol. Geoth. Res. 274, 34–50.

Pichavant, M., Scaillet, B., Pommier, A., Iacono-Marziano, G., Cioni, R., 2014. Nature and evolution of primitive Vesuvius magmas: an experimental study. J. Petrol. 55, 2281–2310.

Pross, J., Koutsodendris, A., Christanis, K., Fischer, T., Fletcher, W.J., Hardiman, M., Kalaitzidis, S., Knipping, M., Kotthoff, U., Milner, A. M., Müller, U.C., Schmiedl, G., Siavalas, G., Tzedakis, P. C. and Wulf, S., 2015. The 1.35-Ma-long terrestrial climate archive of Tenaghi Philippon, northeastern Greece: Evolution, exploration and perspectives for future research. Newsletters on Stratigraphy 48, 253–276.

Railsback, R. B., Gibbard, P. L., Head, M. J., Voarintsoa, N. R. G., Toucanne, S., 2015. An optimized scheme of lettered marine isotope substages for the last 1.0 million years, and the climatostratigraphic nature of isotope stages and substages, Quat. Sci. Rev. 111, 94–106.

Regattieri, E., Giaccio, B., Zanchetta, G., Drysdale, R.N., Galli, P., Nomade, S., Peronace, E., Wulf, S., 2015. Hydrological variability over the Apennines during the Early Last Glacial precession minimum, as revealed by a stable isotope record from Sulmona basin, Central Italy. Journal of Quaternary Science 30, 19–31.

Regattieri, E., Giaccio, B., Galli, P., Nomade, S., Peronace, E., Messina P., Sposato, A., Boschi, C., Gemelli, M. A multi-proxy record of MIS 11-12 deglaciation and glacial MIS 12 instability from the Sulmona Basin (central Italy). Quaternary Science Reviews 132, 129–145.

Regattieri, E., Zanchetta, G., Drysdale, R.N., Isola, I., Hellstrom, J.C., Roncioni, A. 2014. A continuous stable isotope record from the penultimate glacial maximum to the Last Interglacial (159–121 ka) from Tana Che Urla Cave (Apuan Alps, central Italy). Quaternary Research 82, 450-461.

Rouchon, V., Gillot, P.Y., Quidelleur, X., Chiesa, S., Floris, B., 2008. Temporal evolution of the Roccamonfina volcanic complex (Pleistocene), central Italy. Journal of Volcanology and Geothermal Research 177, 500–514.

Sadori, L., Koutsodendris, A., Masi, A., Bertini, A., Combourieu-Nebout, N., Francke, A., Kouli, K., Joannin, S., Mercuri, A.M., Panagiotopoulos, K., Peyron, O., Torri, P., Wagner, B., Zanchetta, G., Donders, T.H., 2015. Pollen-based paleoenvironmental and palaeoclimatic change at Lake Ohrid (SE Europe) during the past 500 ka. Biogeosciences Discussion 12, 15461–15493.

Sagnotti, L., Giaccio, B., Liddicoat, J.C., Nomade, S., Renne, P.R., Scardia, G., Sprain, C.J., 2016. How fast was the Matuyama-Brunhes geomagnetic reversal? A new subcentennial record from the Sulmona Basin, central Italy. Geophysical Journal International 204, 798–812.

Sagnotti, L., Scardia, G., Giaccio, B., Liddicoat, J.C., Nomade, S., Renne, P.R., Sprain C.J., 2014. Extremely rapid directional change during Matuyama-Brunhes geomagnetic polarity reversal, Geophysical Journal International 199, 1110–1124.

Sánchez Gõni, M.E., Turon, J.-L., Eynaud, F., Shackleton, N.J., 1999.High resolution palynological record off the Iberian margin: Direct land–sea correlation for the Last Interglacial complex. Earth and Planetary Science Letters 171, 123–137.

Santacroce, R., Bertagnini, A., Civetta, L., Landi, P, Sbrana, A., 1993. Eruptive dynamics and petrogenetic processes in a very shallow magma reservoir: the 1906 eruption of Somma-Vesuvius. Journal of Petrology 34, 383–425.

Santacroce, R., Cioni, R., Marianelli, P., Sbrana, A., Sulpizio, R., Zanchetta, G., Donahue, D. J., and Joron, J.L., 2008. Age and whole rock–glass compositions of proximal pyroclastics from the major explosive eruptions of -Somma-Vesuvius: A review as a tool for distal tephrostratigraphy. J. Volcanol. Geoth. Res. 177, 1-18.

Sbrana, A., Toccaceli, R.M., 2011. Geological Map of "Isola di Ischia", 1:10000 Scale, Foglio 464. Regione Campania-Assessorato difesa del suolo, Firenze.

Scarpati, C., Perrotta, A., Lepore, S., Calvert, A., 2013. Eruptive history of Neapolitan volcanoes: Constraints from ^{40}Ar-^{39}Ar dating. Geological Magazine, 150, 412–425.

Schmidt, R., Van Den Bogaard, C., Merkt, J., Müller, J., 2002. A new Lateglacial chronostratigraphic tephra marker for the south-eastern Alps: the Neapolitan Yellow Tuff (NYT) in Längsee (Austria) in the context of a regional biostratigraphy and palaeoclimate. Quat. Int. 88, 45-56.

Scholz, D., Hoffmann, D.L., 2011. StalAge – An algorithm designed for construction of speleothem age models. Quaternary Geochronology 6, 369–382.

Shea, T., Larsen, J. F., Gurioli, L., Hammer, J. E., Houghton, B. F., Cioni, R.,2009. Leucite crystals: surviving witnesses of magmatic processes preceding the 79AD eruption at Vesuvius, Italy. Earth and Planetary Science Letters 281, 88-98.

Siani, G., Paterne, M., Michel, E., Sulpizio, R., Sbrana, A., Arnold, M., Haddad, G., 2001. Mediterranean Sea Surface Radiocarbon Reservoir Age Changes Since the Last Glacial Maximum. Science 294, 1917–1920.

Siani, G., Sulpizio, R., Paterne, M., Sbrana, A., 2004. Tephrostratigraphy study for the last 18,000 ^{14}C years in a deep-sea sediment sequence for the South Adriatic. Quat. Sci. Rev. 23, 2485–2500.

Smith, V.C., Isaia, R., Pearce, N.J.G., 2011. Tephrostratigraphy and glass compositions of post-15 kyr Campi Flegrei eruptions: Implications for eruption history and chronostratigraphic markers. Quaternary Science Reviews 25/26, 3638–3660.

Sottili, G., Arienzo I., Castorina, F., Gaeta, M., Giaccio, B., Marra, F., Palladino, D.M., submitted. Sr and Nd isotope signatures during the evolution of the ultrapotassic Sabatini Volcanic District (Roman Province, central Italy), Lithos.

Sottili, G., Taddeucci, J., Palladino, D.M., Gaeta, M., Scarlato, P., Ventura, G., 2009. Sub-surface dynamics and eruptive styles of maars in the Colli Albani volcanic district, central Italy. Journal of Volcanology and Geothermal Research 180, 189–202.

Sottili, G., Palladino, D.M., Marra, F., Jicha, B., Karner, D.B., Renne, P., 2010. Geochronology of the most recent activity in the Sabatini volcanic district, roman province, central Italy. Journal of Volcanology and Geothermal Research 196, 20–30.

Sottili, G., Palladino, D.M., Gaeta, M., Masotta, M., 2012. Origins and energetics of maar volcanoes: examples from the ultrapotassic Sabatini Volcanic District (Roman Province, Central Italy). Bulletin of Volcanology 74, 163–186.

Steiger, R.H., Jäger, E., 1977. Subcommission on geochronology: convention on the use of decay constants in geo-and cosmochronology. Earth and Planetary Science Letters 36, 359-362. Sulpizio, R., Zanchetta, G., D'Orazio, M., Vogel, H., Wagner, B., 2010. Tephrostratigraphy and tephrochronology of lakes Ohrid and Prespa, Balkans. Biogeosciences 7, 3273–3288.

Tamburrino S, Insinga DD, Sprovieri M, Petrosino P, Tiepolo M. 2012. Major and trace element characterization of tephra layers offshore Pantelleria island: Insights into the last 200 ka of volcanic activity and contribution to the Mediterranean tephrochronology. Journal of Quaternary Science 27, 129–140.

Tomlinson, E.L., Albert, P.G., Wulf, S., Brown, R.J., Smith, V.C., Keller, J., Orsi, G., Bourne, A.J., Menzies, M.A., 2014. Age and geochemistry of tephra layers from Ischia, Italy: constraints from proximal-distal correlations with Lago Grande di Monticchio. J. Volcanol. Geotherm. Res. 287, 22-39.

Tomlinson, E.L., Arienzo, I., Civetta, L., Wulf, S., Smith, V.C., Hardiman, M.S., Lane, C.S., Carandente, A., Orsi, G., Rosi, M., Muller, W., Menzies, M.A., 2012. Geochemistry of the Phlegraean Fields (Italy) proximal sources for major Mediterranean tephras: Implications for the dispersal of Plinian and co-ignimbritic components of explosive eruptions. Geochimica et Cosmochimica Acta 93,102–128.

Tzedakis, P.C., Hooghiemstra, H., Pälike, H., 2006. The last 1.35 million years at Tenaghi Philippon: revised chronostratigraphy and long-term vegetation trends. Quaternary Science Reviews 25, 3416–3430.

Villa, V., Pereira, A., Chaussé, C., Nomade, S., Giaccio, B., Limondin-Lozouet, N., Fusco, F., Regattieri, E., Degeai, J.-., Robert, V., Kuzucuoglu, C., Boschian, G., Agostini, S., Aureli, D., Pagli, M., Bahain, J.J., Nicoud, E., 2016. A MIS 15-MIS 12 record of environmental changes and Lower Palaeolithic occupation from Valle Giumentina, central Italy. Quaternary Science Reviews 151, 160–184.

Wagner, B., Wilke, T., Krastel, S., Zanchetta, G., Sulpizio, R., Reicherter, K., Leng, M., Grazhdani, A., Trajanovski, S., Levkov, Z., Reed, J., Wonik, T. 2014. More than one million years of history in Lake Ohrid cores. Eos 95, 25-26.

Wulf, S., Kraml, M., Keller, J., 2008. Towards a detailed distal tephrostratigraphy in the Central Mediterranean: the last 20,000 yrs record of Lago Grande di Monticchio. Journal of Volcanology and Geothermal Research 177, 118–132.

Watts, W.A., Allen, J.R.M. Huntley, B., 1996. Vegetation history and palaeoclimate of the last glacial period of Lago Grande di Monticchio, southern Italy, Quaternary Science Reviews 15, 133–153.

Wulf, S., Keller, J., Paterne, M., Mingram, J., Lauterbach, S., Opitz, S., Sottili, G., Giaccio, B., Albert, P.G, Satow, C., Tomlinson, E.L., Viccaro, M., Brauer, A., 2012. The 100-133 ka record of Italian explosive volcanism and revised tephrochronology of Lago Grande di Monticchio. Quaternary Science Reviews 58, 104–123.

Wulf, S., Kraml, M., Keller, J., Negendank, J.F.W., 2004. Tephrochronology of the 100 ka lacustrine sediment record of Lago Grande di Monticchio (southern Italy). Quaternary International 122, 7–30.

Zanchetta, G., Regattieri, E., Giaccio, B., Wagner, B., Sulpizio, R., Francke, A., Vogel, L. H., Sadori, L., Masi, A., Sinopoli, G., Lacey, J. H., Leng, M. L., and Leicher, N.: Aligning MIS5 proxy records from Lake Ohrid (FYROM) with independently dated Mediterranean archives: implications for core chronology. Biogeosciences 13, 2757–2768, doi:10.5194/bg-13-2757-2016.

Zanchetta, G., Sulpizio, R., Giaccio, B., Siani, G., Paterne, M., Wulf, S., D'Orazio, M., 2008. The Y-3 tephra: a Last Glacial stratigraphic marker for the central Mediterranean basin. Journal of Volcanology and Geothermal Research 177, 145–154.

Zanchetta, G., Sulpizio, R., Roberts, N., Cioni, R., Eastwood, W.J., Siani, G., Caron, B., Paterne, M., Santacroce, R., 2011. Tephrostratigraphy, chronology and climatic events of the Mediterranean basin during the Holocene: an overview. The Holocene 21, 33–52.

Table and figure captions

Table 1. Sr and Nd isotope compositions of glass or feldspar (*) form the investigated Fucino tephra and from some of their potential correlatives from Sulmona Basin (POP1 and POP2) and Lake Ohorid (OH-DP-0624).

Table 2. Volcanic sources of the investigated tephra.

Figure 1. Reference maps of the Fucino Plain with a representative seismic line. **(a)** Location of the Fucino Basin with respect to the main volcanic districts of the central and southern Italy. **(b)** Location of the investigated Fucino 1-3 (F1-F3), SP and SPE cores and of the quoted GeoLazio (GL) and Telespazio (TS) cores in the Fucino plain. The isochrones of the Plio-Quaternary basin infilling, the Quaternary master faults responsible for the asymmetrical (half-graben) geometry of the basin and the epicenter of the last strong earthquake (A.D. 1915) are also shown. **(c)** Seismic line 3 (see trace in panel b) showing the internal architecture of the Plio-Quaternary continental deposits of the Fucino Basin along a W-E-oriented profile. The projected location of the GL, SP, SPE and F1-F3 boreholes is also shown. A, B, C: main unconformities; Seq. 2: Messinian foredeep sediments; Seq.3: Pliocene fluvial-alluvial deposits; Seq. 4: Quaternary lacustrine-fluvial deposits. Figure and information are compiled with some modifications from Cavinato et al. (2002), Galli et al. (2012), and Patacca et al. (2008).

Figure 2. Tephrostratigraphy, selected proxy data and $^{40}Ar/^{39}Ar$ ages of the investigated F1-F3, SP and SPE cores. **(a)** Tephrostratigraphic correlation between the cores (refer to Fig. 1 for core location) showing the progressive eastward increase of the tephra depths – i.e., toward the basin depocenter – as depicted by the seismic data (Fig. 1). **(b)** K, Rb, Sr and Ca from XRF scanning and low-resolution $\delta^{18}O_{TIC}$ in core F1-F3 (Giaccio et al., 2015b). **(c)** Composite tephrostratigraphy, the results of the direct $^{40}Ar/^{39}Ar$ dating, presented in this study, are also shown. **(d)** Pictures of some representative tephra in core F1-F3. Blue/yellow shadowing indicates marine isotope stages (MIS) following the correlation proposed in Giaccio et al. (2015b). The type of the analyses (WDS-EMPA, LA-ICP-AMS, Sr-Nd composition and $^{40}Ar/^{39}Ar$ dating) and their distribution among tephra from the three cores are also shown.

Figure 3. Representative major and trace element compositions for the Fucino tephra. **(a)** Total alkali versus silica classification diagram (Le Maitre, 2002) of the Fucino tephras compared with compositional field of the volcanic deposits from selected Italian volcanoes that were active during the late Middle Pleistocene-Holocene period. Data sources; Colli Albani (glass-WDS): Marra et al. (2009), Gaeta et al. (2011), Giaccio et al. (2013a), Cross et al. (2014); Somma-Vesuvius (glass-EDS): Santacroce et al. (2008); Somma-Vesuvius (glass-WDS): Tomlinson et al. (2015); Vulsini-Sabatini-Vico (glass-WDS): Palladino et al. (2014), Marra et al. (2014); Vulsini-Sabatini-Vico-Roccamonfina (whole rock-XRF): Peccerillo (2005 and references therein), Perini et al. (2008), Rouchon et al. (2008); Campi Flegrei (glass-WDS): Smith et al. (2011), Tomlinson et al. (2012); Ischia (glass-WDS): Tomlinson et al. (2014); Etna (whole rock-XRF) Peccerillo (2005 and references therein). The compositions of the glasses have been recalculated to 100 wt% on an anhydrous basis. **(b)** Incompatible trace element bi-plots comparing the Fucino glasses from tephra TF-12, TF-13 and TF-17 with those erupted at Campi Flegrei (Tomlinson et al., 2012) and Ischia (Tomlinson et al., 2014) all within the last 100 kyr (2σ standard deviations of replicate LA-ICP-MS analyses of the StHs6/80-G MPI-DING glass standard are not shown here as the uncertainties are smaller than the data symbols).

Figure 4. Sr vs Nd isotopes of products from the Roman and the Campanian magmatic Province are plotted, together with the analyzed Fucino tephra samples. Literature data (D'Antonio et al., 2007, 2013, Brown et al., 2014; Direnzo et al., 2007; Di Renzo et al., 2011; Conticelli et al., 1997, 2009; Boari et al., 2009a, 2009b;

Del Bello et al., 2014; Gaeta et al., 2016; Sottili et al., submitted) have been plotted as reference fields. The fields circumscribe and include all the individual data. Vertical line corresponds the $^{87}Sr/^{86}Sr$ isotope ratios of the TF 7 sample. Tephra associated to volcanic eruptions from Neapolitan area or Roman Province can be distinguished by Sr and Nd isotope fingerprintings. The effect of alteration in modifying the Sr isotope composition of sample OH-DP-0624 is also evident. The less fluid mobile Nd element in not affected by alteration and is in the range of volcanic products from the Neapolitan volcanic area.

Figure 5. Age probability density spectra diagrams from tephra TF-4, TF-5, TF-7, TF-14 and TF-17. Blue and red bars indicate the individual ages (1σ error) included and discarded in weighted mean age, respectively.

Figure 6. Cl versus CaO/FeO diagram for the trachyte-phonolite and tephri-phonolite Fucino tephra (SiO_2 content ranging between ~52 wt% and 65 wt%) discriminating their volcanic source. The fields of the individual volcanic sources have been defined on the basis of the composition of glass from proximal pyroclastic successions, with exception of Roccamonfina. For this volcano, in addition to few glass compositions from proximal deposits (this study), we considered the composition of the glass from distal tephra found in Mercure Basin, southern Italy, the attribution of which was proposed on basis of $^{87}Sr/^{86}Sr$ ratio (Giaccio et al., 2014). Data source; Somma-Vesuvius (glass-EDS): Santacroce et al. (2008); Campi Flegrei (glass-WDS): Smith et al. (2011), Tomlinson et al. (2012); Ischia (glass-WDS): Tomlinson et al. (2014); Roccamonfina-Mercure (glass-WDS): Giaccio et al. (2014), this study; Sabatini (glass-WDS): Marra et al. (2014); Vico (glass-WDS): Palladino et al. (2014), Marra et al. (2014); Vulsini: Palladino et al. (2014).

Figure 7. Total alkali versus silica classification diagram and representative bi-plots for the Campi Flegrei TF-1,TF-2, TF-6 and TF-10 (**a, b**, **c** and **d**) Fucino tephra compared with their proximal or distal counterparts. Data source; Campi Flegrei volcanics from the 1st to the 3rd epoch of activity: Smith et al. (2011); proximal Neapolitan Yellow Tuff (NYT) and pre-NYT Tufi Biancastri (glass-WDS): Tomlinson et al. (2012); Matese-NYT (glass-WDS) $^{40}Ar/^{39}Ar$ dated tephra (14.5 ± 0.4 ka): Galli et al. (2016b); Pre-

Campanian Ignimbrite Trefola a-f (pre-CI Tla to Tlf) (glass-WDS): Tomlinson et al. (2012); POP1 (glass-WDS): Giaccio et al. (2012); PRAD2517 (glass-WDS): Bourne et al. (2010).

Figure 8. Total alkali versus silica classification diagram and representative bi-plots for the Fucino tephra TF-11 **(a)**, TF-12 **(b)**, TF-13 **(c)** and TF-17 **(d)** from an undefined source in Neapolitan volcanic area compared with their proximal or distal counterparts. Data source; TM-24a (glass-WDS): Wulf et al. (2004); POP2a and CIL1 (glass-WDS): Giaccio et al. (2012); POP4 (glass-WDS): Regattieri et al. (2015); CIL2 (glass-WDS): Giaccio et al. (2012); TM-27 (glass-WDS): Wulf et al. (2012); t1 (glass-EDS): Iorio et al. (2014); PRAD-2812 (glass-WDS): Bourne et al. (2015); CF-V5 (glass-WDS): Giraudi and Giaccio (2015); OH-DP-0624 (glass-WDS-EDS): Leicher et al. (2016); OT0701-7 (glass-EDS): Sulpizio et al. (2010); PRAD-3225 (glass-WDS): Bourne et al (2015).

Figure 9. Representative trace element concentrations for the Fucino tephra layers TF-12, TF-13 and TF-17 and potential correlatives. **(a)** TF-12 glasses clearly geochemically correspond to X-5 tephra correlatives at Lago Grande di Monticchio (TM-25; Wulf et al., 2012), in the Sulmona Basin (POP3; Wulf et al., 2012; Giaccio et al., 2012) and along the Cilento coastline (CIL1/LeS1; Giaccio et al., 2012; Donato et al., 2016), whilst geochemically differing from the younger MIS 5 tephra deposits at Lago Grande di Monticchio (TM-23-3c, TM-24a, TM-24b; Wulf et al., 2012) and in the Adriatic marine core PRAD 1-2 (PRAD 2525 and PRAD 2605; Bourne et al., 2015). **(b)** TF-13 glasses correspond to the compositionally heterogeneous correlatives of the X-6 tephra. These include reported occurrences of the X-6 along the Cilento coastline (CIL2/LeS2; Giaccio et al., 2012; Donato et al., 2016), in the Valle di Crati, Calabria (Tarsia Tephra; Donato et al., 2016), on Salina Island (Aeolian Islands, southern Tyrrhenian Sea; Albert, 2012), in Lago Grande di Monticchio (TM-27; Wulf et al., 2012; Bourne et al., 2015) and in both Adriatic (PRAD 2812; Bourne et al., 2015) and Ionian Sea (I-9; Insinga et al., 2014) marine cores. **(c)** TF-17 is correlated to the Lake Ohrid tephra, OH-DP-0624 (Leicher et al., 2016). The Fucino tephra TF-17 is dominated by the more evolved phonolitic end-member of this heterogeneous tephra, reflected by analyses showing greater levels of incompatible trace element enrichment, whilst the OH-DP-0624 is dominated by the less evolved phono-tephrite end-member glasses which show lower levels of incompatible trace element enrichment. Error bars

represent 2σ standard deviations of replicate analyses of the StHs6/80-G MPI-DING glass standard, where absent, the error is smaller than the data points presented.

Figure 10. Total alkali versus silica classification diagram and representative bi-plots for the Fucino tephra TF-3a and TF-3b **(a)**, TF-4 and TF-5 **(b)**, TF-8 and TF-9 **(c)** and TF-7 **(d)** compared with their proximal or distal counterparts. Data source; Mezzano and Ionian Sea Y-1 and Biancavilla Giarre fall D1a-D2a and Acireale fall D2b and D1b (glass-WDS): Albert et al. (2013); I-1 and I-a in Ionian Sea core KC01B (glass-WDS): Insinga et al. (2014); Albano 7 (glass-WDS): Giaccio et al. (2013); Albano VII and Albano V (glass-WDS): Cross et al. (2014); CF-V3 (glass-WDS): Giraudi et al. (2011); Albano 1 and Albano 3 (glass-WDS): Gaeta et al. (2011), Freda et al. (2006); Monte Epomeo Green Tuff (glass-WDS): Tomlinson et al. (2014); PRAD-1870 (glass-WDS): Bourne et al. (2010).

Figure 11. Total alkali versus silica classification diagram and representative bi-plots for the Fucino tephra TF-21 **(a)**, TF-14 **(b)**, TF-15 **(d)** and TF-16 **(c)** compared with their proximal or distal counterparts. Data source; Tyrrhenian Sea layers C-52 and C-54 (glass-EDS): Paterne et al. (2008); Sabatini Baccano Lower Unit (BAC-LU) (glass-WDS): this study; Vico C Ignimbrite (glass-WDS): Palladino et al. (2014); Vico B Ignimbrite and CF-V4 (glass-WDS): Giraudi et al. (2011); OH-DP-0617 (glass-WDS-EDS): Leicher et al. (2016).

Figure 12. Volcanic sources, individual correlations and ages of the Fucino tephra and/or of equivalent eruptions/tephra and profile of the Ca content (Giaccio et al., 2015b) of the investigated lacustrine succession. For comparison, the sea surface temperature (SST) record from the western Mediterranean core MD95-2043 (Martrat et al., 2004) is also shown. The boundaries of the marine isotope stages (MIS) and sub-stages (orange and blue bars) in MD95-2043 record are according to Railsback et al. (2015) and are projected in the Fucino record along the intercept points of the yellow/blue bars with the dashed blue line, which is the linear interpolation between the mid-point of the tephra ages. The ages of Fucino tephra (dashed pink lines) are in turn projected in the time-scale of the MD95-2043 record, which is based on its own age

model (see details in Martrat et al., 2004). NYT: Neapolitan Yellow Tuff; MEGT: Monte Epomeo Green Tuff.

Figure 13. Synopsis of the tephra correlations between the Fucino tephra, volcanic sources, individual eruptions and/or equivalent distal tephra from some representative tephrostratigraphic records of the central Mediterranean and Balkans area (N.B., in the latter only Fucino-equivalent tephra are shown). CF: Campi Flegrei; CF?: Neapolitan volcanic area, likely Campi Flegrei; CA: Colli Albani. References; Sulmona: Giaccio et al. (2012), Galli et al. (2015), Regattieri et al. (2015); Campo Felice: Giraudi et al. (2011), Giraudi and Giaccio (2015); Monticchio: Wulf et al. (2004; 2012); San Gregorio Magno: Munno and Petrosino (2007); Adriatic Sea: Bourne et al. (2008; 2015); Siani et al. (2004); Tyrrhenian-Ionian Sea: Paterne et al. (2008), Insinga et al. (2014), Petrosino et al. (2016); Lake Ohrid: Leicher et al (2016).

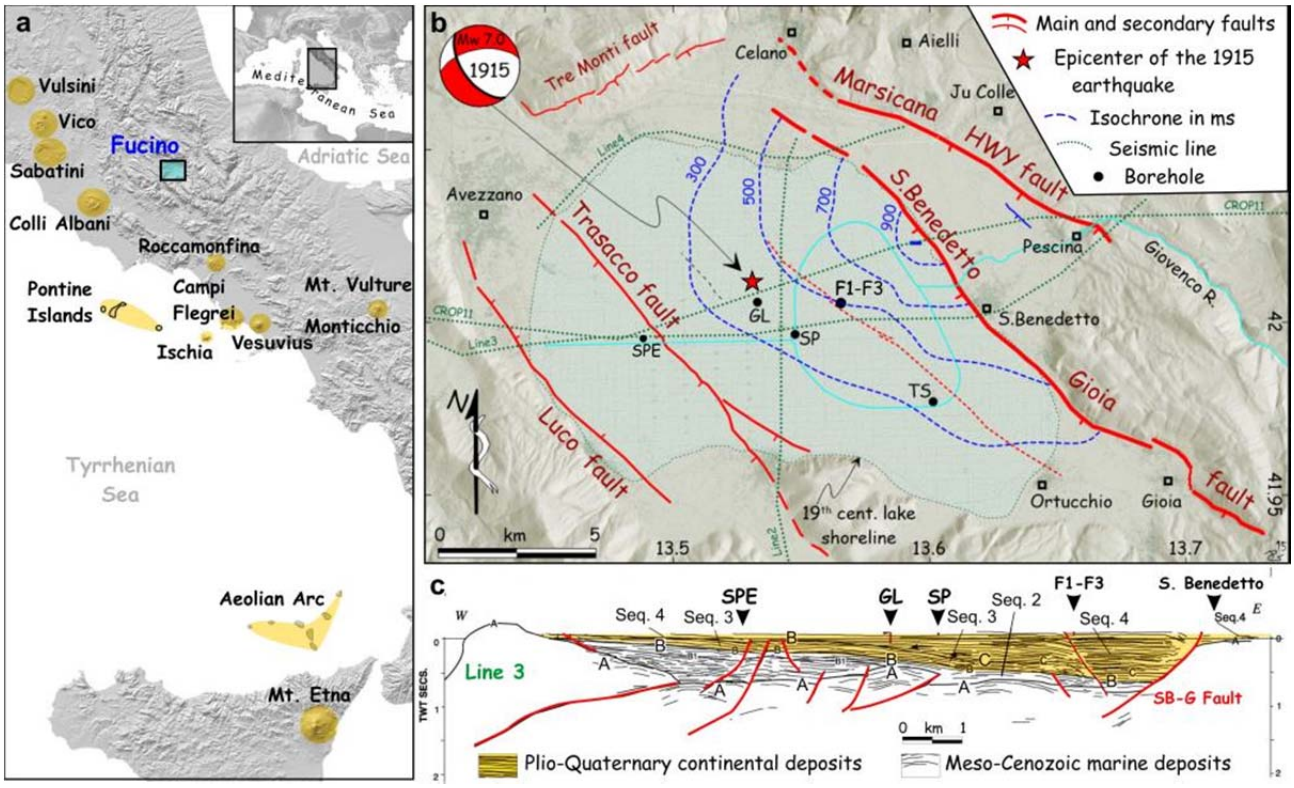
a
Vulsini
Vico
Fucino
Sabatini
Colli Albani
Roccamonfina
Pontine Islands
Campi Flegrei
Mt. Vulture
Monticchio
Vesuvius
Ischia
Tyrrhenian Sea
Adriatic Sea
Aeolian Arc
Mt. Etna
b
Mw 7.0
1915
Tre Monti fault
Celano
Aielli
Ju Colle
Marsicana HWY fault
S.Benedetto
Avezzano
Trasacco fault
Pescina
Giovenco R.
F1-F3
GL
SP
SPE
S.Benedetto
TS
Gioia
Luco fault
Ortucchio
Gioia
Fault
19th cent. lake shoreline
0 km 5
13.5
13.6
13.7
42
41.95
Main and secondary faults
Epicenter of the 1915 earthquake
Isochrone in ms
Seismic line
Borehole
c
Line 3
SPE
GL
SP
F1-F3
S. Benedetto
Seq. 4
Seq. 3
Seq. 2
SB-G Fault
0 km 1
Plio-Quaternary continental deposits
Meso-Cenozoic marine deposits

Fig. 1

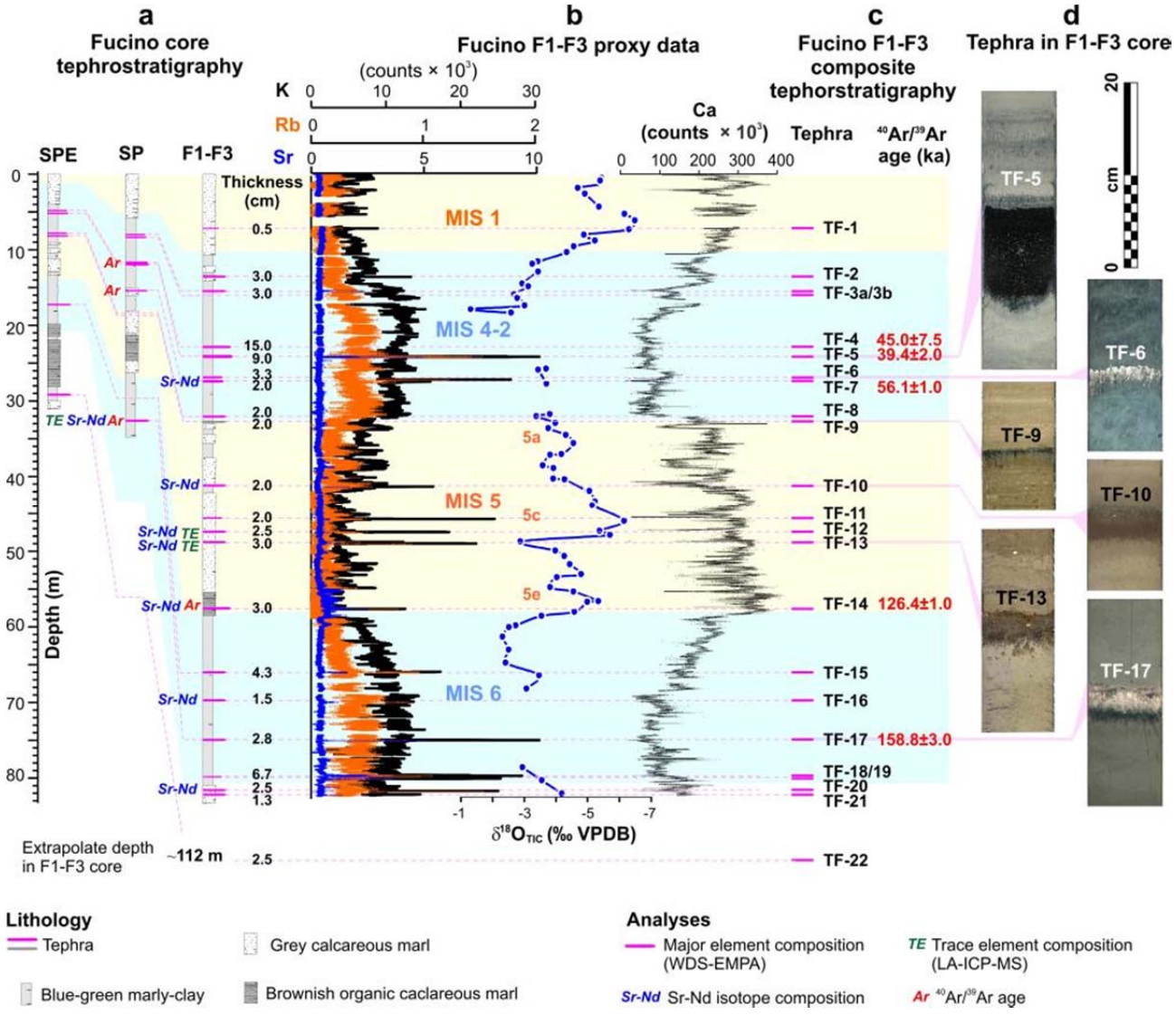
a
Fucino core tephrostratigraphy
b
Fucino F1-F3 proxy data
c
Fucino F1-F3 composite tephorstratigraphy
d
Tephra in F1-F3 core
SPE
SP
F1-F3
Thickness (cm)
Depth (m)
K (counts × 10³)
Rb
Sr
Ca (counts × 10³)
Tephra
⁴⁰Ar/³⁹Ar age (ka)
MIS 1
MIS 4-2
MIS 5
MIS 6
5a
5c
5e
TF-1
TF-2
TF-3a/3b
TF-4 45.0±7.5
TF-5 39.4±2.0
TF-6
TF-7 56.1±1.0
TF-8
TF-9
TF-10
TF-11
TF-12
TF-13
TF-14 126.4±1.0
TF-15
TF-16
TF-17 158.8±3.0
TF-18/19
TF-20
TF-21
TF-22
Extrapolate depth in F1-F3 core
~112 m
δ¹⁸O_TIC (‰ VPDB)
cm
Lithology
Tephra
Grey calcareous marl
Blue-green marly-clay
Brownish organic caclareous marl
Analyses
Major element composition (WDS-EMPA)
TE Trace element composition (LA-ICP-MS)
Sr-Nd Sr-Nd isotope composition
Ar ⁴⁰Ar/³⁹Ar age

Fig. 2

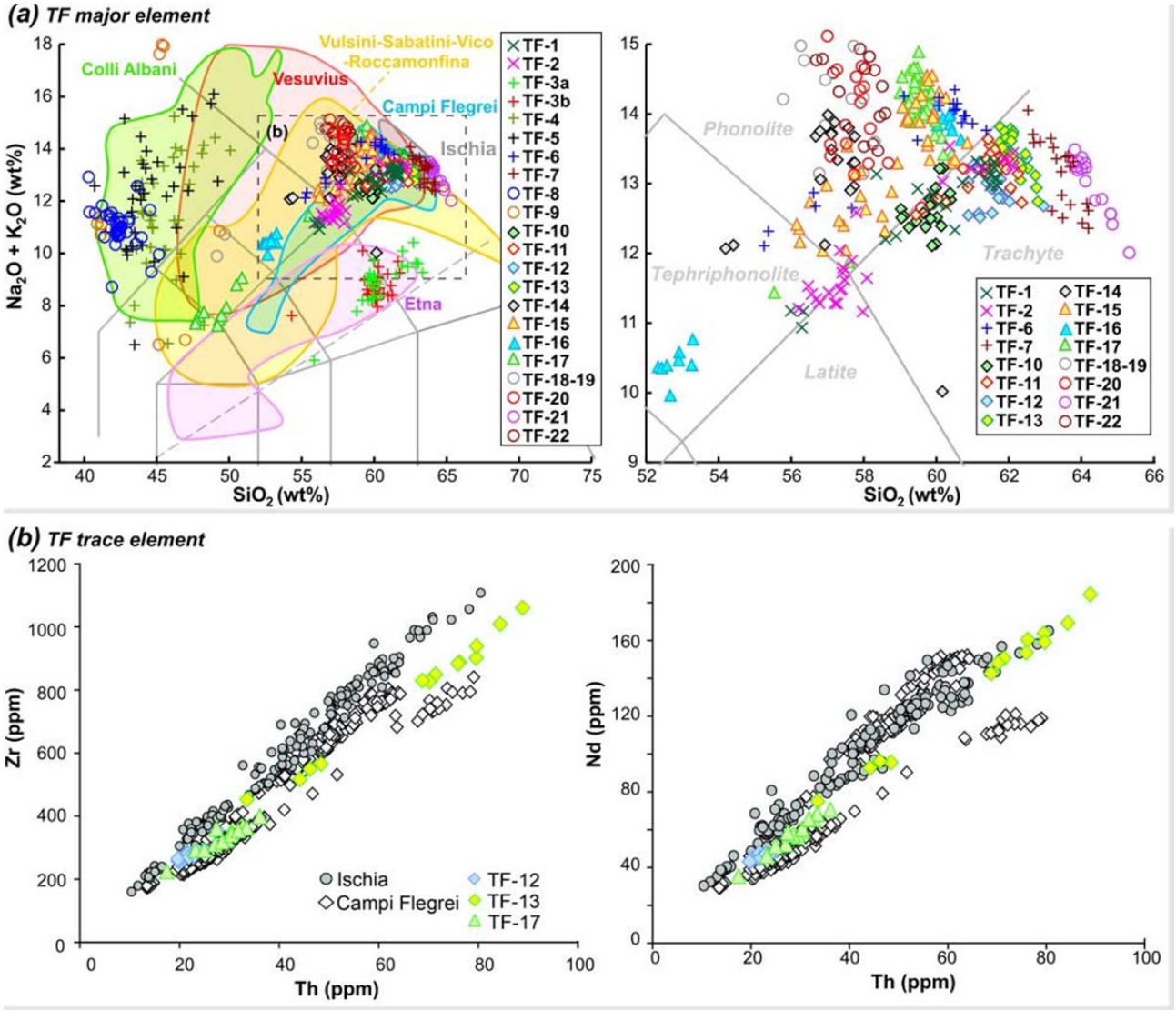
(a) TF major element
Colli Albani
Vulsini-Sabatini-Vico
-Roccamonfina
Vesuvius
Campi Flegrei
Ischia
Etna
(b)
TF-1
TF-2
TF-3a
TF-3b
TF-4
TF-5
TF-6
TF-7
TF-8
TF-9
TF-10
TF-11
TF-12
TF-13
TF-14
TF-15
TF-16
TF-17
TF-18-19
TF-20
TF-21
TF-22
Na2O + K2O (wt%)
SiO2 (wt%)
Phonolite
Trachyte
Tephriphonolite
Latite
(b) TF trace element
Zr (ppm)
Th (ppm)
Nd (ppm)
Ischia
Campi Flegrei

Fig. 3

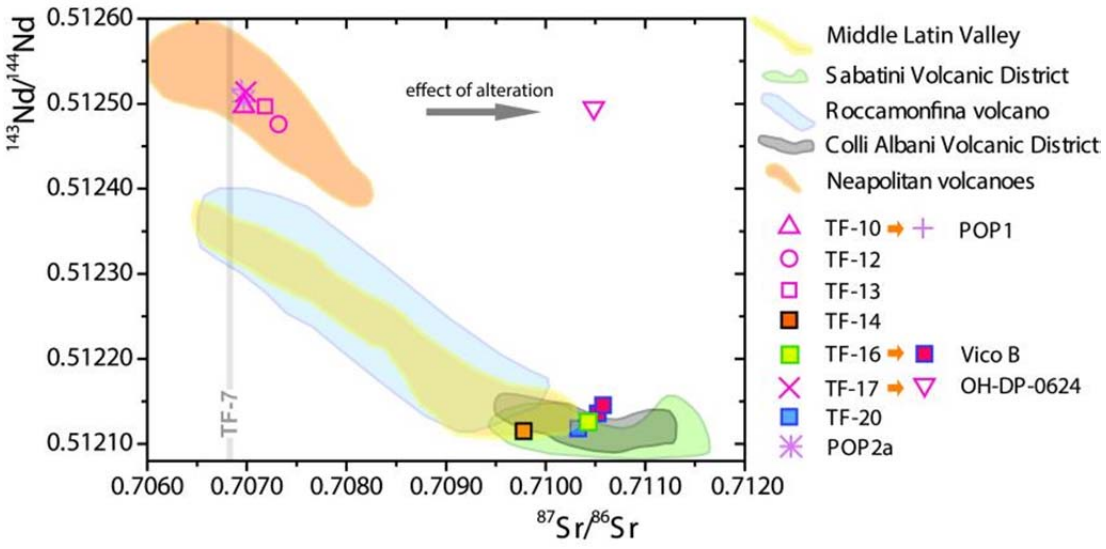
effect of alteration
TF-7
143Nd/144Nd
87Sr/86Sr
Middle Latin Valley
Sabatini Volcanic District
Roccamonfina volcano
Colli Albani Volcanic District
Neapolitan volcanoes
TF-10
POP1
TF-12
TF-13
TF-14
TF-16
Vico B
TF-17
OH-DP-0624
TF-20
POP2a

Fig. 4

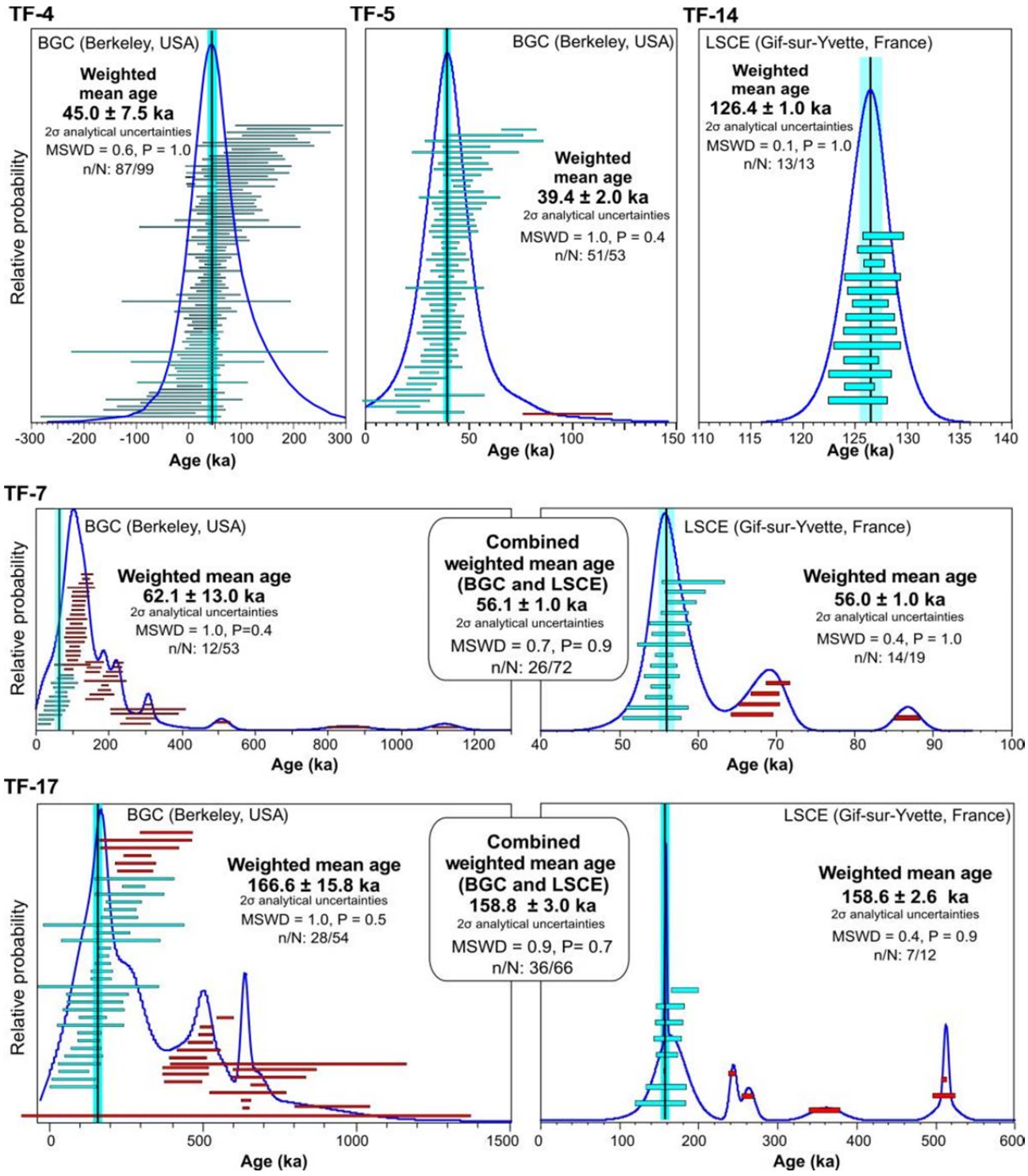
TF-4
BGC (Berkeley, USA)
Weighted mean age
45.0 ± 7.5 ka
2σ analytical uncertainties
MSWD = 0.6, P = 1.0
n/N: 87/99
Relative probability
Age (ka)
TF-5
BGC (Berkeley, USA)
Weighted mean age
39.4 ± 2.0 ka
2σ analytical uncertainties
MSWD = 1.0, P = 0.4
n/N: 51/53
Age (ka)
TF-14
LSCE (Gif-sur-Yvette, France)
Weighted mean age
126.4 ± 1.0 ka
2σ analytical uncertainties
MSWD = 0.1, P = 1.0
n/N: 13/13
Age (ka)
TF-7
BGC (Berkeley, USA)
Weighted mean age
62.1 ± 13.0 ka
2σ analytical uncertainties
MSWD = 1.0, P=0.4
n/N: 12/53
Combined weighted mean age (BGC and LSCE)
56.1 ± 1.0 ka
2σ analytical uncertainties
MSWD = 0.7, P= 0.9
n/N: 26/72
LSCE (Gif-sur-Yvette, France)
Weighted mean age
56.0 ± 1.0 ka
2σ analytical uncertainties
MSWD = 0.4, P = 1.0
n/N: 14/19
Relative probability
Age (ka)
TF-17
BGC (Berkeley, USA)
Weighted mean age
166.6 ± 15.8 ka
2σ analytical uncertainties
MSWD = 1.0, P = 0.5
n/N: 28/54
Combined weighted mean age (BGC and LSCE)
158.8 ± 3.0 ka
2σ analytical uncertainties
MSWD = 0.9, P= 0.7
n/N: 36/66
LSCE (Gif-sur-Yvette, France)
Weighted mean age
158.6 ± 2.6 ka
2σ analytical uncertainties
MSWD = 0.4, P = 0.9
n/N: 7/12
Relative probability
Age (ka)

Fig. 5

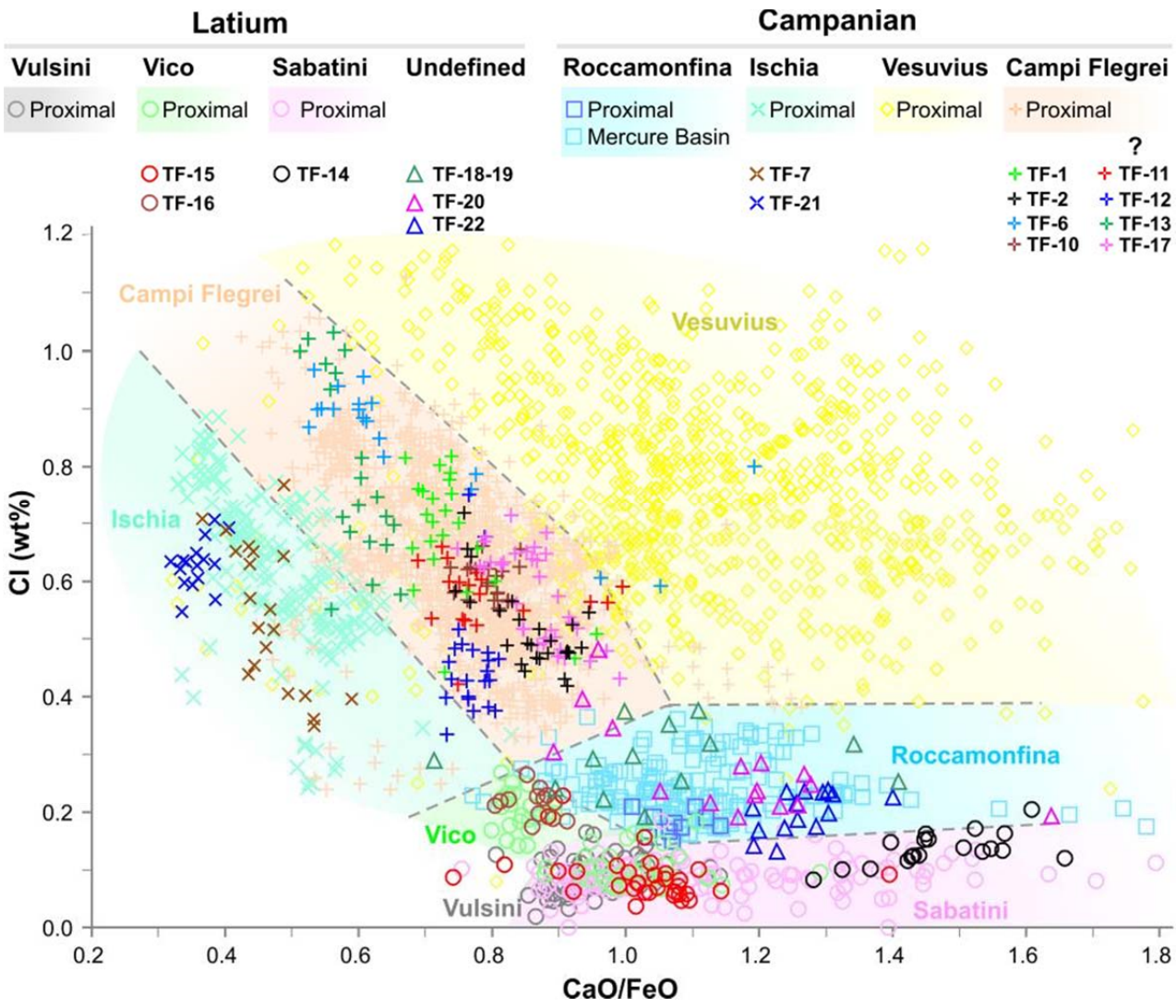
Latium
Campanian
Vulsini
Vico
Sabatini
Undefined
Roccamonfina
Ischia
Vesuvius
Campi Flegrei
Proximal
Mercure Basin
TF-15
TF-16
TF-14
TF-18-19
TF-20
TF-22
TF-7
TF-21
?
TF-1
TF-2
TF-6
TF-10
TF-11
TF-12
TF-13
TF-17
Campi Flegrei
Vesuvius
Ischia
Roccamonfina
Vico
Vulsini
Sabatini
Cl (wt%)
CaO/FeO
0.0
0.2
0.4
0.6
0.8
1.0
1.2
1.4
1.6
1.8

Fig. 6

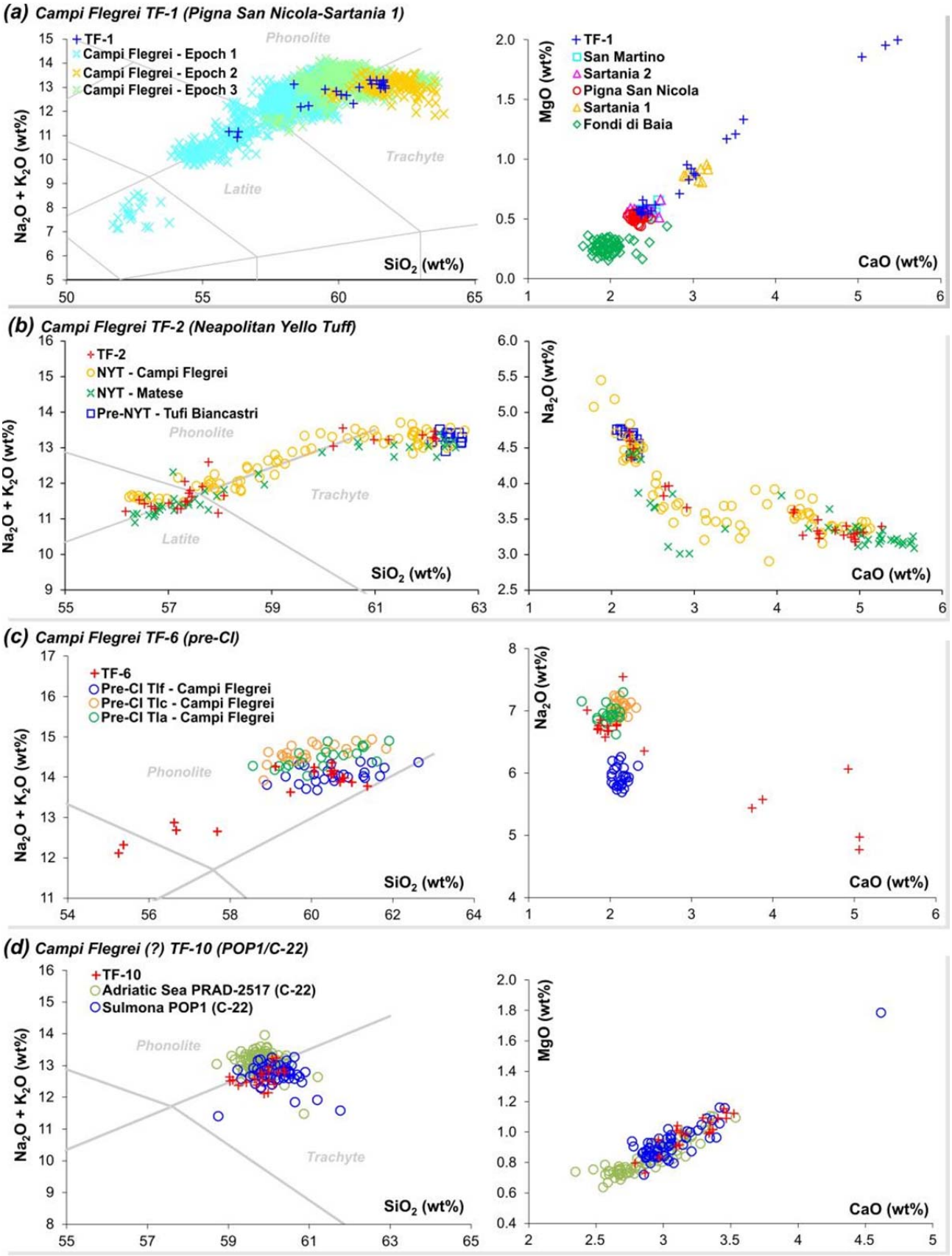
(a) Campi Flegrei TF-1 (Pigna San Nicola-Sartania 1)
TF-1
Campi Flegrei - Epoch 1
Campi Flegrei - Epoch 2
Campi Flegrei - Epoch 3
Phonolite
Trachyte
Latite
Na2O + K2O (wt%)
SiO2 (wt%)
TF-1
San Martino
Sartania 2
Pigna San Nicola
Sartania 1
Fondi di Baia
MgO (wt%)
CaO (wt%)
(b) Campi Flegrei TF-2 (Neapolitan Yello Tuff)
TF-2
NYT - Campi Flegrei
NYT - Matese
Pre-NYT - Tufi Biancastri
Phonolite
Trachyte
Latite
Na2O + K2O (wt%)
SiO2 (wt%)
Na2O (wt%)
CaO (wt%)
(c) Campi Flegrei TF-6 (pre-CI)
TF-6
Pre-CI Tlf - Campi Flegrei
Pre-CI Tlc - Campi Flegrei
Pre-CI Tla - Campi Flegrei
Phonolite
Na2O + K2O (wt%)
SiO2 (wt%)
Na2O (wt%)
CaO (wt%)
(d) Campi Flegrei (?) TF-10 (POP1/C-22)
TF-10
Adriatic Sea PRAD-2517 (C-22)
Sulmona POP1 (C-22)
Phonolite
Trachyte
Na2O + K2O (wt%)
SiO2 (wt%)
MgO (wt%)
CaO (wt%)

Fig. 7

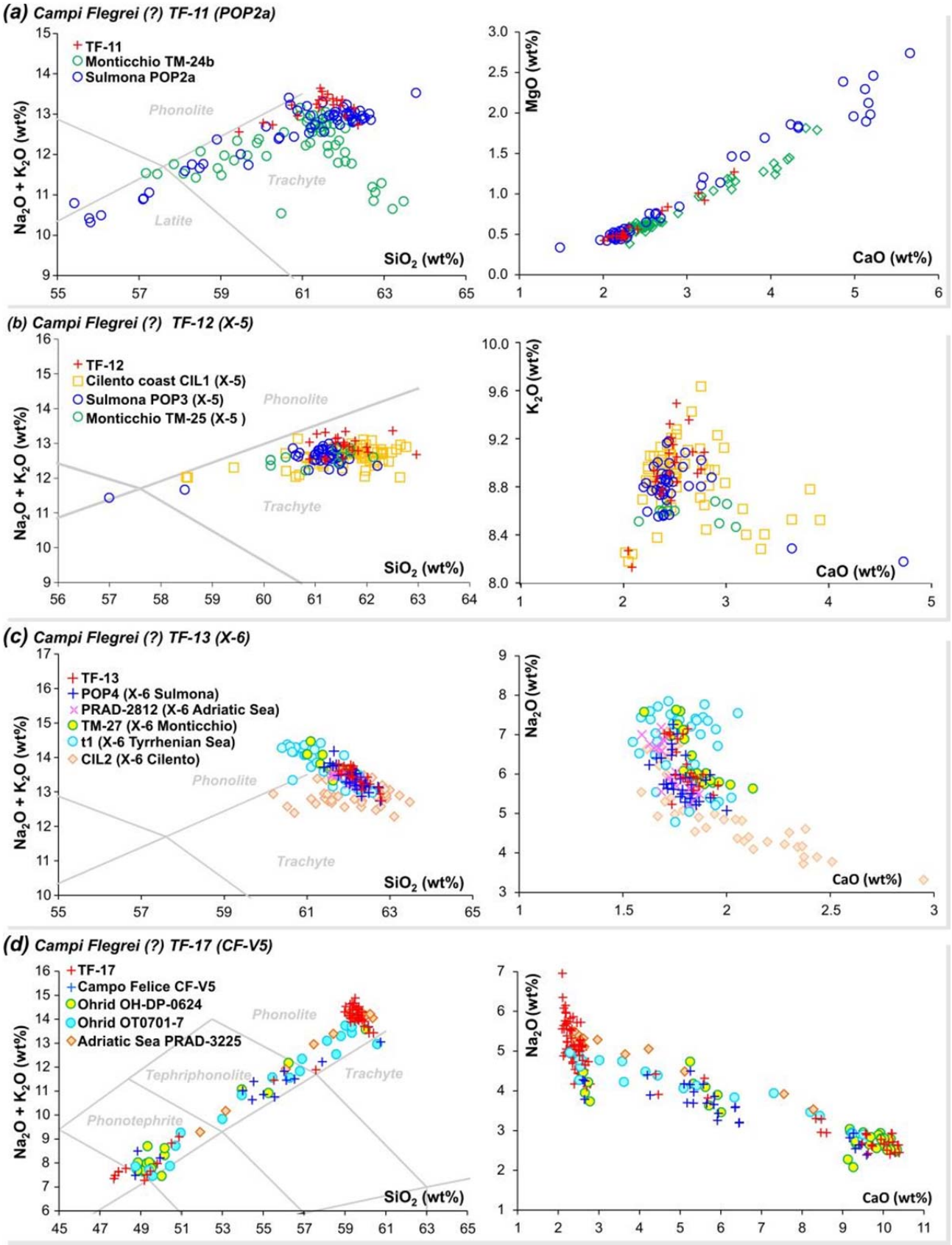
(a) Campi Flegrei (?) TF-11 (POP2a)
TF-11
Monticchio TM-24b
Sulmona POP2a
Phonolite
Trachyte
Latite
Na2O + K2O (wt%)
SiO2 (wt%)
MgO (wt%)
CaO (wt%)
(b) Campi Flegrei (?) TF-12 (X-5)
TF-12
Cilento coast CIL1 (X-5)
Sulmona POP3 (X-5)
Monticchio TM-25 (X-5)
Phonolite
Trachyte
Na2O + K2O (wt%)
SiO2 (wt%)
K2O (wt%)
CaO (wt%)
(c) Campi Flegrei (?) TF-13 (X-6)
TF-13
POP4 (X-6 Sulmona)
PRAD-2812 (X-6 Adriatic Sea)
TM-27 (X-6 Monticchio)
t1 (X-6 Tyrrhenian Sea)
CIL2 (X-6 Cilento)
Phonolite
Trachyte
Na2O + K2O (wt%)
SiO2 (wt%)
Na2O (wt%)
CaO (wt%)
(d) Campi Flegrei (?) TF-17 (CF-V5)
TF-17
Campo Felice CF-V5
Ohrid OH-DP-0624
Ohrid OT0701-7
Adriatic Sea PRAD-3225
Phonolite
Tephriphonolite
Trachyte
Phonotephrite
Na2O + K2O (wt%)
SiO2 (wt%)
Na2O (wt%)
CaO (wt%)

Fig. 8

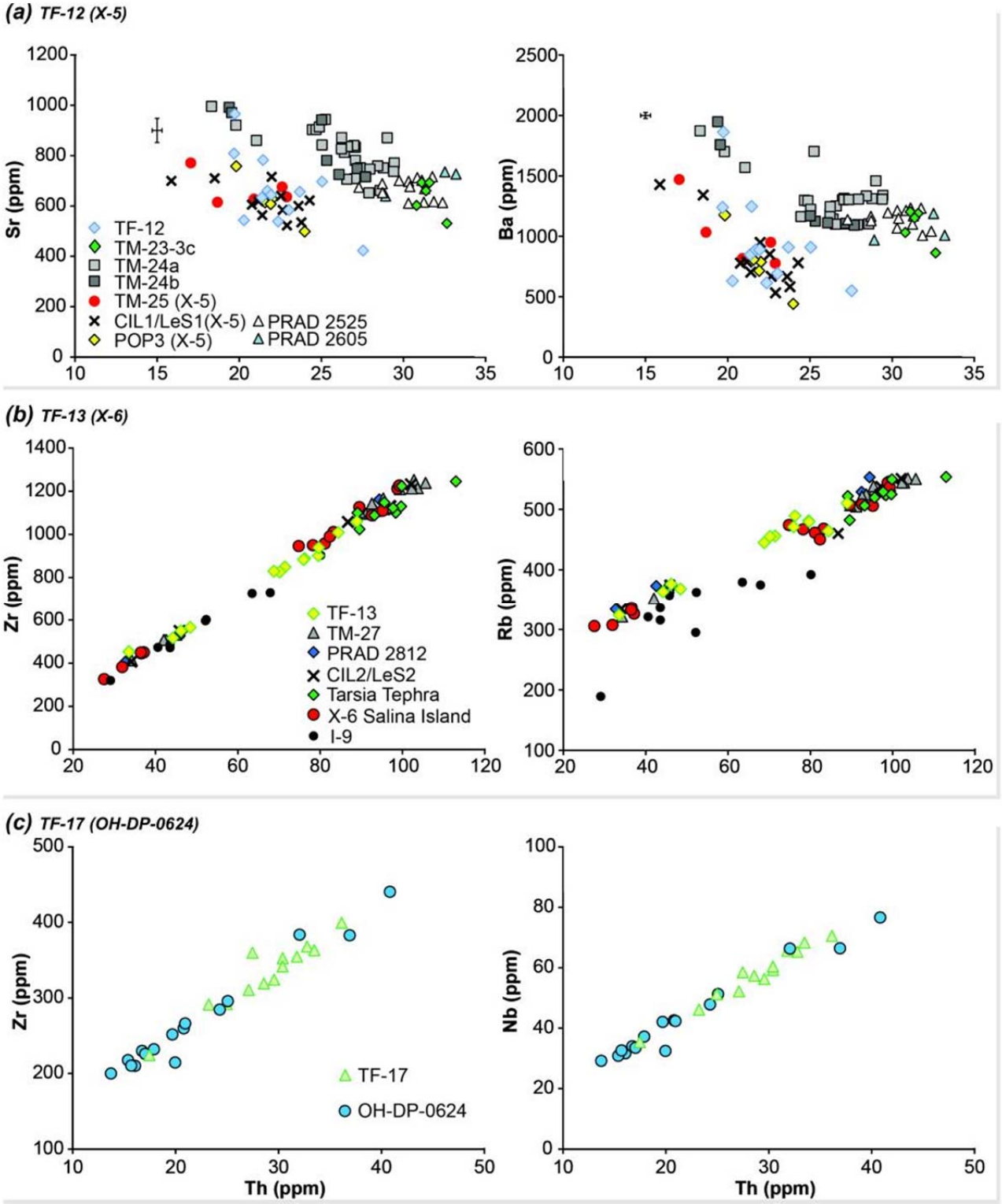
(a) TF-12 (X-5)
Sr (ppm)
Ba (ppm)
TF-12
TM-23-3c
TM-24a
TM-24b
TM-25 (X-5)
CIL1/LeS1(X-5)
POP3 (X-5)
PRAD 2525
PRAD 2605
(b) TF-13 (X-6)
Zr (ppm)
Rb (ppm)
TF-13
TM-27
PRAD 2812
CIL2/LeS2
Tarsia Tephra
X-6 Salina Island
I-9
(c) TF-17 (OH-DP-0624)
Zr (ppm)
Nb (ppm)
TF-17
OH-DP-0624
Th (ppm)
Th (ppm)

Fig. 9

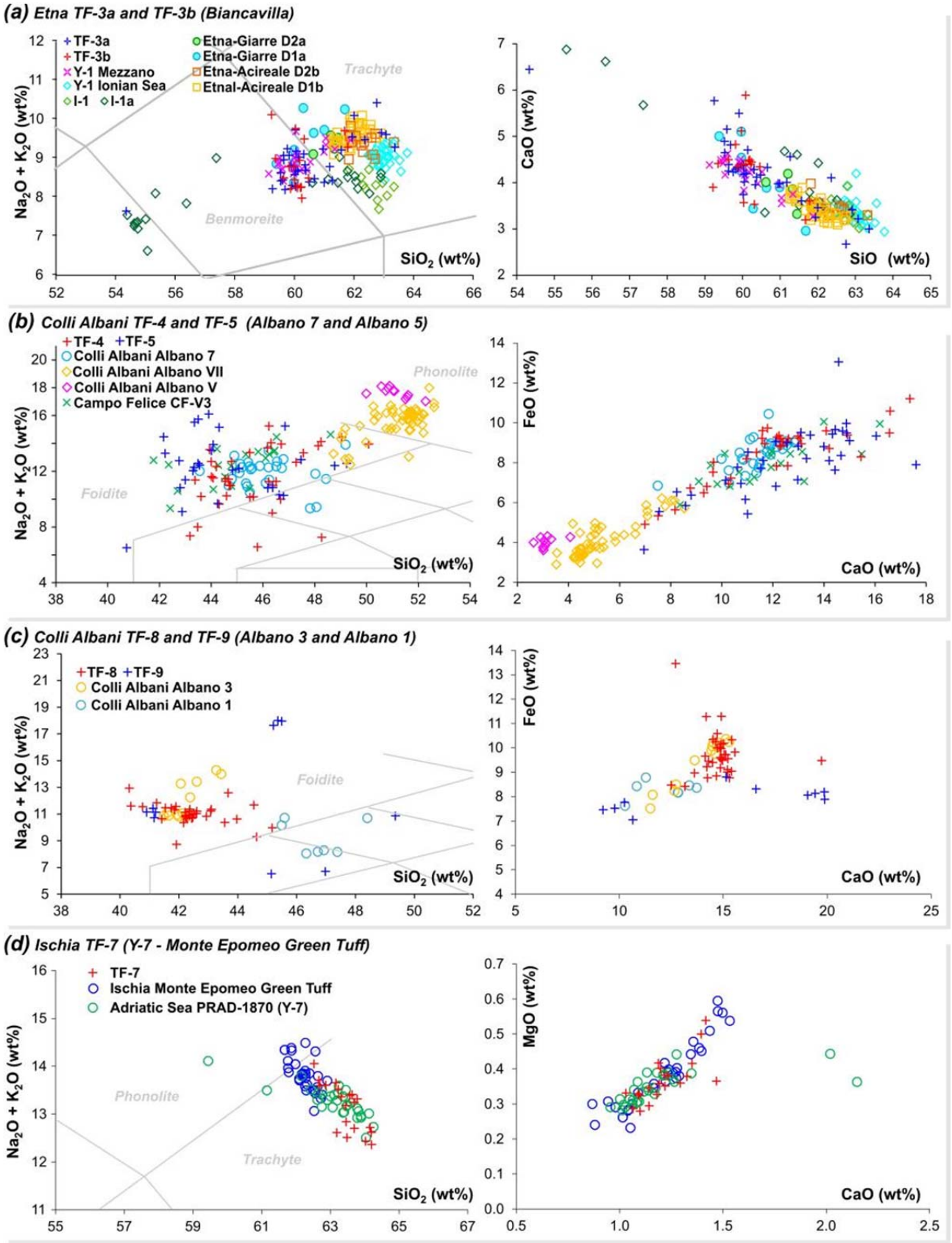
(a) Etna TF-3a and TF-3b (Biancavilla)
TF-3a
TF-3b
Y-1 Mezzano
Y-1 Ionian Sea
I-1
I-1a
Etna-Giarre D2a
Etna-Giarre D1a
Etna-Acireale D2b
Etnal-Acireale D1b
Trachyte
Benmoreite
Na2O + K2O (wt%)
SiO2 (wt%)
CaO (wt%)
SiO (wt%)
(b) Colli Albani TF-4 and TF-5 (Albano 7 and Albano 5)
TF-4
TF-5
Colli Albani Albano 7
Colli Albani Albano VII
Colli Albani Albano V
Campo Felice CF-V3
Phonolite
Foidite
FeO (wt%)
CaO (wt%)
(c) Colli Albani TF-8 and TF-9 (Albano 3 and Albano 1)
TF-8
TF-9
Colli Albani Albano 3
Colli Albani Albano 1
(d) Ischia TF-7 (Y-7 - Monte Epomeo Green Tuff)
TF-7
Ischia Monte Epomeo Green Tuff
Adriatic Sea PRAD-1870 (Y-7)
MgO (wt%)

Fig. 10

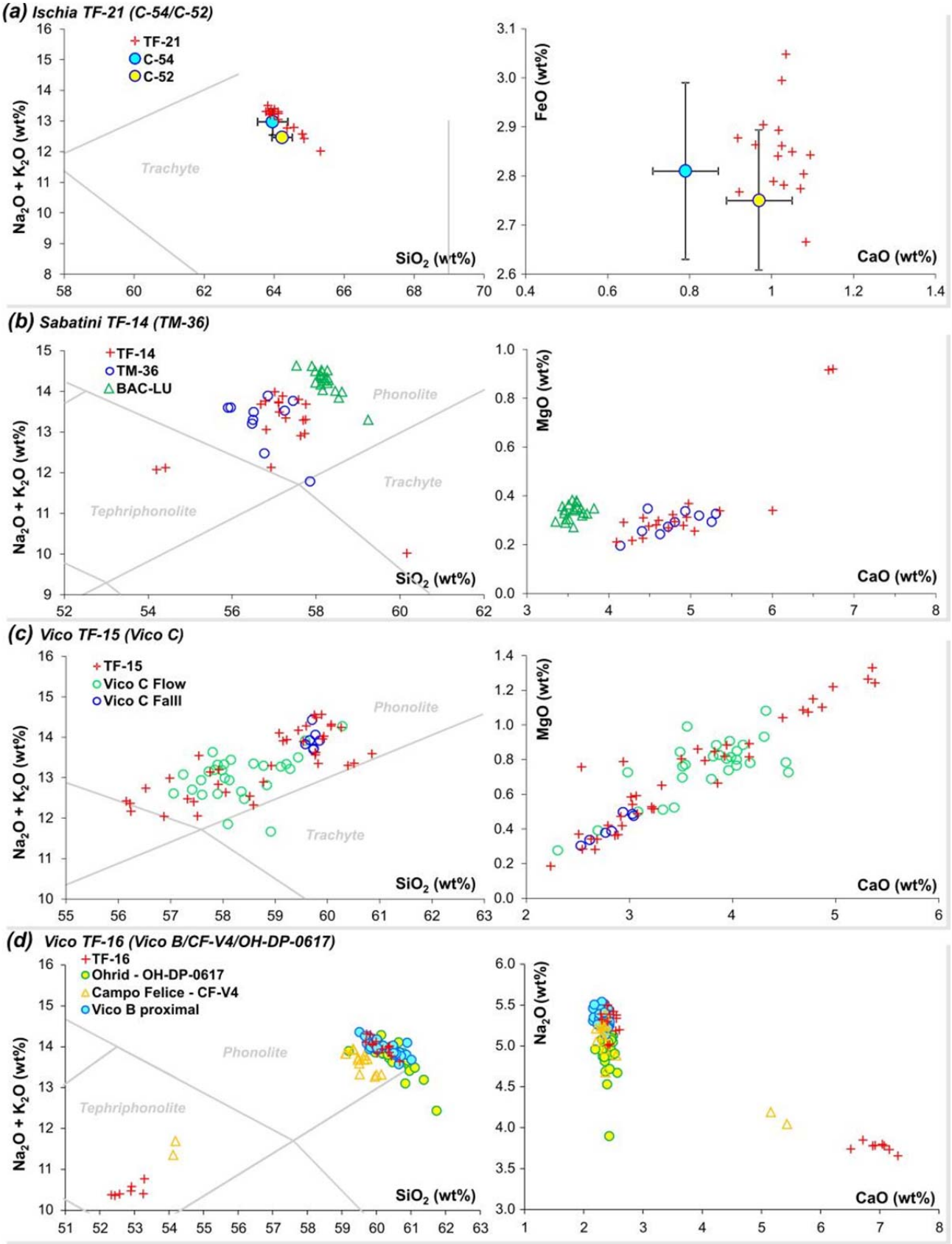
(a) Ischia TF-21 (C-54/C-52)
TF-21
C-54
C-52
Trachyte
Na2O + K2O (wt%)
SiO2 (wt%)
FeO (wt%)
CaO (wt%)
(b) Sabatini TF-14 (TM-36)
TF-14
TM-36
BAC-LU
Phonolite
Trachyte
Tephriphonolite
MgO (wt%)
(c) Vico TF-15 (Vico C)
TF-15
Vico C Flow
Vico C FallI
(d) Vico TF-16 (Vico B/CF-V4/OH-DP-0617)
TF-16
Ohrid - OH-DP-0617
Campo Felice - CF-V4
Vico B proximal
Na2O (wt%)

Fig. 11

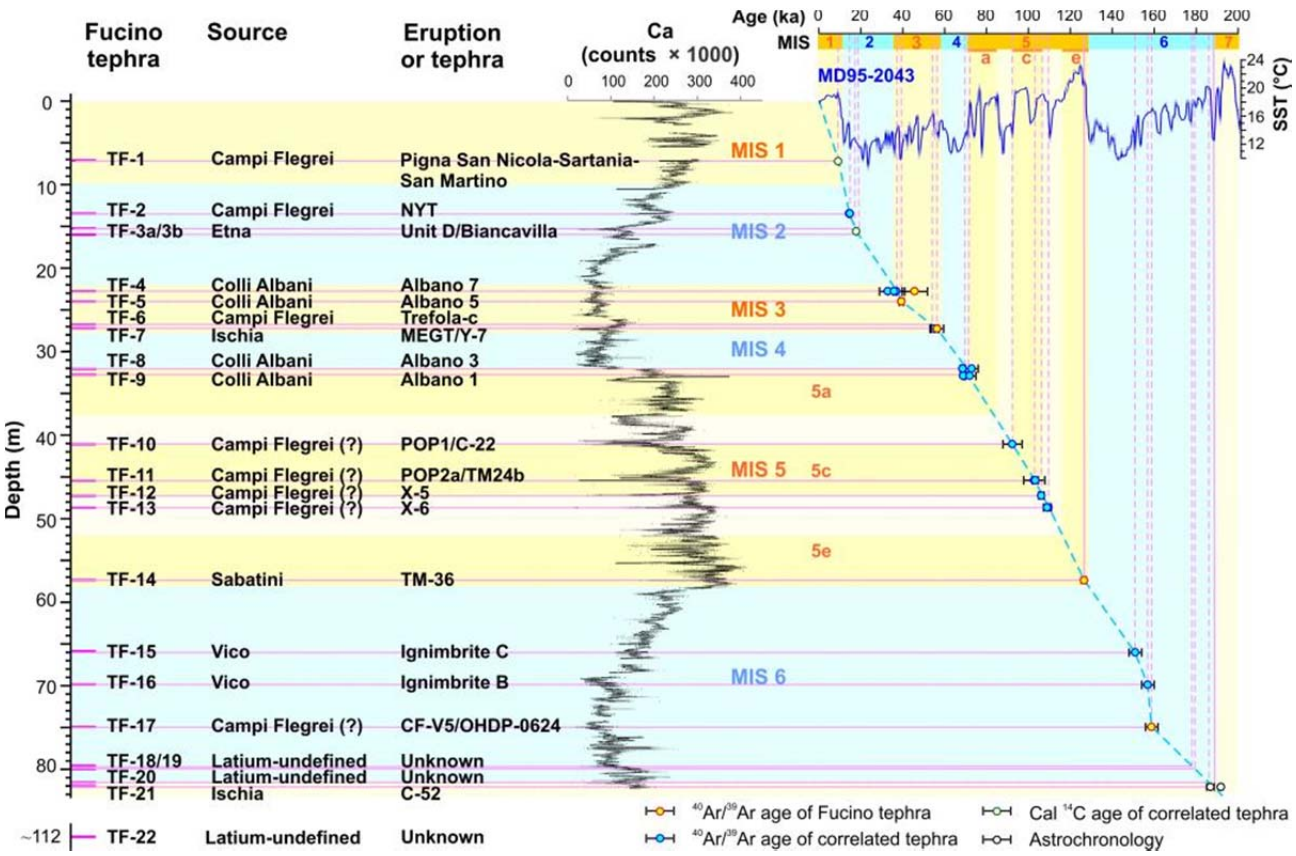
Fucino tephra
Source
Eruption or tephra
Ca (counts × 1000)
Age (ka)
MIS
MD95-2043
SST (°C)
Depth (m)
TF-1 Campi Flegrei Pigna San Nicola-Sartania-San Martino
TF-2 Campi Flegrei NYT
TF-3a/3b Etna Unit D/Biancavilla
TF-4 Colli Albani Albano 7
TF-5 Colli Albani Albano 5
TF-6 Campi Flegrei Trefola-c
TF-7 Ischia MEGT/Y-7
TF-8 Colli Albani Albano 3
TF-9 Colli Albani Albano 1
TF-10 Campi Flegrei (?) POP1/C-22
TF-11 Campi Flegrei (?) POP2a/TM24b
TF-12 Campi Flegrei (?) X-5
TF-13 Campi Flegrei (?) X-6
TF-14 Sabatini TM-36
TF-15 Vico Ignimbrite C
TF-16 Vico Ignimbrite B
TF-17 Campi Flegrei (?) CF-V5/OHDP-0624
TF-18/19 Latium-undefined Unknown
TF-20 Latium-undefined Unknown
TF-21 Ischia C-52
~112 TF-22 Latium-undefined Unknown
MIS 1
MIS 2
MIS 3
MIS 4
5a
MIS 5
5c
5e
MIS 6
40Ar/39Ar age of Fucino tephra
40Ar/39Ar age of correlated tephra
Cal 14C age of correlated tephra
Astrochronology

Fig. 12

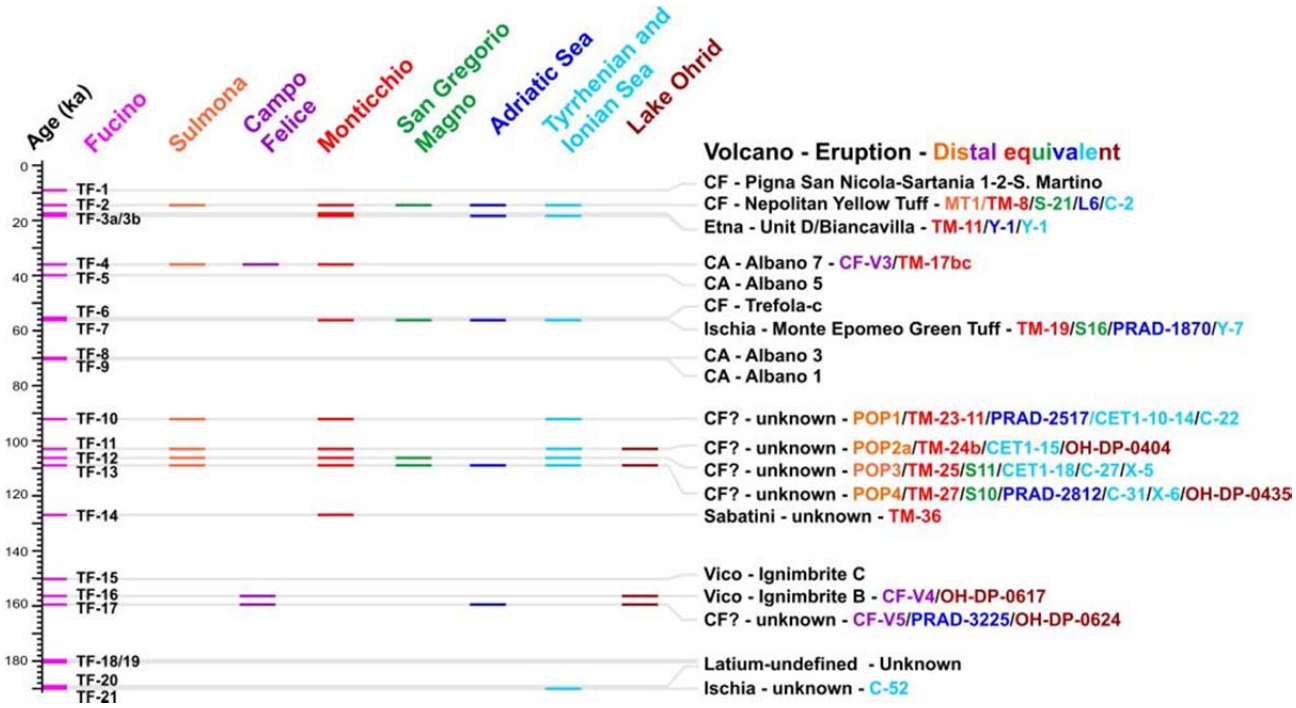
Age (ka)
Fucino
Sulmona
Campo Felice
Monticchio
San Gregorio Magno
Adriatic Sea
Tyrrhenian and Ionian Sea
Lake Ohrid
Volcano - Eruption - Distal equivalent
TF-1
TF-2
TF-3a/3b
TF-4
TF-5
TF-6
TF-7
TF-8
TF-9
TF-10
TF-11
TF-12
TF-13
TF-14
TF-15
TF-16
TF-17
TF-18/19
TF-20
TF-21
CF - Pigna San Nicola-Sartania 1-2-S. Martino
CF - Nepolitan Yellow Tuff - MT1/TM-8/S-21/L6/C-2
Etna - Unit D/Biancavilla - TM-11/Y-1/Y-1
CA - Albano 7 - CF-V3/TM-17bc
CA - Albano 5
CF - Trefola-c
Ischia - Monte Epomeo Green Tuff - TM-19/S16/PRAD-1870/Y-7
CA - Albano 3
CA - Albano 1
CF? - unknown - POP1/TM-23-11/PRAD-2517/CET1-10-14/C-22
CF? - unknown - POP2a/TM-24b/CET1-15/OH-DP-0404
CF? - unknown - POP3/TM-25/S11/CET1-18/C-27/X-5
CF? - unknown - POP4/TM-27/S10/PRAD-2812/C-31/X-6/OH-DP-0435
Sabatini - unknown - TM-36
Vico - Ignimbrite C
Vico - Ignimbrite B - CF-V4/OH-DP-0617
CF? - unknown - CF-V5/PRAD-3225/OH-DP-0624
Latium-undefined - Unknown
Ischia - unknown - C-52

Fig. 13

Analysed tephra	$^{87}Sr/^{86}Sr_{TQ}$	$^{87}Sr/^{86}Sr_{purified}$	$^{143}Nd/^{144}Nd$	Analysed tephra	$^{87}Sr/^{86}Sr$	$^{143}Nd/^{144}Nd$	Volcanic source	Main correlatives
TF-7		0.706846*					Ischia	Y-7
TF-10	0.706973	n.a.	0.512497	**POP1**	0.706948	0.512517	Campi Flegrei?	C-22
TF-11	n.a.	n.a.		**POP2a**	0.706969	0.512503	Campi Flegrei?	TM-24b
TF-12	0.707318	n.a.	0.512476				Campi Flegrei?	X-5
TF-13	0.707241	0.707183	0.512497				Campi Flegrei?	X-6
TF-14	0.709781	n.a.	0.512115				Sabatini	
TF-17	0.707093	0.706988	0.512514	**OH-DP-0624**	0.710483	0.512495	Campi Flegrei?	PRAD 3225
TF-16		0.710428	0.512128				Vico	Vico B
TF-20		0.710327	0.512118				Latium-undefined	

Table 1

Tephra	Campi Flegrei	Neapolitan undefined (>60 ka)	Mt. Etna	Colli Albani	Ischia	Sabatini	Vico	Latium undefined
TF-1								
TF-2								
TF-3a								
TF-3b								
TF-4								
TF-5								
TF-6								
TF-7								
TF-8								
TF-9								
TF-10								
TF-11								
TF-12								
TF-13								
TF-14								
TF-15								
TF-16								
TF-17								
TF-18/19								
TF-20								
TF-21								
TF-22								

Table 2